An Earth Model Based on Free Oscillations and Body Waves

DON L. ANDERSON AND ROBERT S. HART

Seismological Laboratory, California Institute of Technology
Pasadena, California 91125

Several recent inversion studies have clearly indicated the lack of resolving power of the normal mode data set and the possible trade-offs among the various parameters. These studies have also shown that the final model is as dependent on the starting model as on the data set. It is therefore important to incorporate body wave data into any inversion scheme not only to gain resolution but also to reduce trade-offs between density and velocity. An earth model based on special studies of the structure of the mantle and core is inverted to be consistent with both body wave data and a representative set of normal mode observations (437 modes). The resulting model has a 40-km-thick upper mantle lithospheric lid terminating at 61 km, with high density (3.5 g/cm^3) and seismic velocities (8.38 and 4.71 km/s), a pronounced upper mantle low-velocity zone (LVZ) of 180-km thickness, and transition regions of rapid velocity increase at 375–425, 500–550, and 650–675 km. There are also anomalous gradients between 700 and 1200 km. This model, C2, is slow by about 0.6 and 2–4 s for P and S waves, respectively, in comparison with body wave solutions which have a greater continental bias. The major features of the upper mantle can be explained by partial melting (LVZ) and the successive transformation of an olivine-pyroxene mantle to β spinel, γ spinel, and garnet and further phase changes below 750 km. In addition to the radial inhomogeneities in the upper mantle there is evidence for inhomogeneity at the base of the mantle, the top of the core, and the regions on each side of the outer core–inner core boundary.

INTRODUCTION

The normal mode data set is now adequate to determine average velocities and densities in the upper and lower mantle and the core and to resolve a certain amount of structure in these regions. However, it is not adequate to resolve details having wavelengths of the order of 100–200 km. To resolve these features, which are particularly important in the upper mantle and the transition regions of the mantle and core, one must utilize body wave techniques, which are of a higher resolving power, including travel times, apparent velocities, amplitudes, and pulse shapes. These data by their nature and availability are more path dependent than normal modes, but it is reasonable to assume that the fine structure determined by body wave techniques is largely characteristic of the earth as a whole. The role of free oscillations then is to determine differences of the average earth from the more path specific body wave structures and to determine compatible density structures. In this spirit, we design a starting model based on high-resolution body wave studies and perturb this model to fit the normal mode data set. The resulting model retains the features found by body wave studies, but the average properties in the various regions are suitably adjusted to correspond to average earth properties, as is required by the normal mode data set. This model is appropriate for discussions of gross earth chemistry and as a standard for discussing lateral variations.

Jordan and Anderson [1974] recently derived an earth model consistent with a large body of free oscillation, surface wave, and body wave data. These data tightly constrain the seismic velocities and densities in the lower mantle and outer core. However, the resolving power in the upper mantle and transition region, particularly for P waves, is very poor, and the resulting model, as in all studies of this sort, is to a large extent dependent on the starting model. Although model B1, derived by *Jordan and Anderson* [1974], fit the available gross earth data, it has several unsatisfactory features. The upper mantle compressional velocity structure, because of the resolving power problem, appears to be inconsistent with the shear velocity profile, which can be resolved to greater detail. In particular, the low P_n velocity, 7.91 km/s, is inconsistent with both the high S_n velocity, 4.83 km/s, and the measurements of P_n in oceanic and most continental regions. Model B1 has no P wave low-velocity layer in the upper mantle, but it does have a rather pronounced low-velocity zone (LVZ) for shear waves. Resolving power calculations indicate that an upper mantle P wave LVZ cannot be resolved by the normal mode data set even though detailed body wave studies demonstrate its existence in most parts of the earth.

The low P_n velocity and the absence of a P wave LVZ are related problems, since only average properties of the upper mantle can be determined. If one accepts the P_n data, then inversion of the same data set would yield a P wave LVZ. Model B1 also gives shear wave travel times that are not consistent with recent studies [*Hart*, 1975; *Hales and Roberts*, 1970].

Recent body wave studies of the upper mantle using travel times, amplitudes, and wave shapes [*Helmberger and Wiggins*, 1971; *Helmberger and Engen*, 1974] have yielded profiles having more structure than can probably ever be resolved from gross earth data. These structures include LVZ's for both P and S waves and discontinuities near 375, 500, and 600 km. Gradients between discontinuities, as well as average velocities, can also be resolved with these techniques. Although the above studies refer mostly to continental structure below North America, there is reason to believe that the major features also exist elsewhere. For example, evidence for the 375- and 600-km discontinuities appears in great circle, mainly oceanic, dispersion data [e.g., *Anderson and Toksöz*, 1963] and from upper mantle reflection studies [e.g., *Engdahl and Flinn*, 1969; *Whitcomb and Anderson*, 1970]. Evidence for the 500-km discontinuity has also been discussed for oceanic regions [*Whitcomb and Anderson*, 1970] and for Australia [*Simpson*, 1973].

The interpretation of these discontinuities in terms of phase changes [*Anderson*, 1967*a*, *b*; *Burdick and Anderson*, 1975] requires that they occur everywhere, although their depths may vary slightly.

It seems appropriate therefore to adopt the high-resolution

body wave profiles as starting models in a gross earth inversion, and to allow them to be modified as necessary to satisfy the gross earth data. We make no pretense that the fine structure in the starting and final models is required by the normal mode data set.

THE STARTING MODEL

The basic starting model is a modification of the *Helmberger and Wiggins* [1971] and *Helmberger and Engen* [1974] structures for the upper mantle, B1 for the lower mantle, and B1 and *Whitcomb* [1973] for the core. *Whitcomb* [1973] constructed his core model from observed $dt/d\Delta$'s, relative amplitudes, and arrival times of *PKP*, *PKiKP*, *SKS*, and *SKKS*, utilizing a recent mantle model [*Jordan and Anderson*, 1974] for the required stripping to the surface of the core. He discusses at length previous core studies. A crust and uppermost mantle model was derived which is an average of the tectonic subdivisions of the earth. It includes a 3-km-thick water layer in order to overcome the objections of *Hales* [1974]. It has a 40-km-thick lid (the mantle part of the lithosphere), a 58-km-thick lithosphere, pronounced low-velocity zones for both *P* and *S*, and discontinuities or rapid increases in velocity, near 375, 500, and 670 km. The latter discontinuity was made sharp in order to satisfy *P'P'* precursor reflection data [*Engdahl and Flinn*, 1969; *Whitcomb and Anderson*, 1970].

Model B1 of *Jordan and Anderson* [1974] represented the 'shortest smooth perturbation' from a simple initial model that incorporated the major seismic discontinuities (400 and 600 km) found from previous body wave and surface wave studies [*Anderson and Toksöz*, 1963; *Niazi and Anderson*, 1965; *Julian and Anderson*, 1968; *Johnson*, 1967] and that upon inversion satisfied the normal mode data set of *Dziewonski and Gilbert* [1972] and a large body of supplementary data including travel times, apparent velocities, and group velocities. The starting model had an adiabatic and homogeneous lower mantle and outer core. The starting, or initial, model for the present study incorporates fine structure of the upper mantle [*Helmberger and Wiggins*, 1971; *Helmberger and Engen*, 1974], uppermost lower mantle [*Hart*, 1975], and core [*Whitcomb*, 1973] which is unresolvable by the normal mode data set. In addition, we modified the starting V_p model to be consistent with the P_n data. The starting density model contains discontinuities in the upper mantle at the depths of the seismic discontinuities.

It should be emphasized that in linear inversion the starting model is as important as the data set. Our starting model incorporates features found by techniques which have an intrinsic greater resolving power than the gross earth data set itself. The inversion technique that we used is identical to that described by *Jordan and Anderson* [1974]. For the forward part of the calculations we used programs written by Martin Smith. The radius of the core was fixed at 3485 km, the value determined by *Jordan and Anderson* [1974] and verified by *Engdahl and Johnson* [1974]. This core radius is also consistent with the solutions of *Hales and Roberts* [1970] and *Gilbert and Dziewonski* [1975]. It is about 12 km larger than earlier determinations, such as that of *Jeffreys and Bullen* [1940], but agrees with one of the solutions of *Hales and Roberts* [1970].

As a first step we inverted the toroidal mode data for shear velocity and density, thus removing the coupling between V_p and V_s. We then inverted using a combination of toroidal modes and the spheroidal modes that are particularly sensitive to shear velocity, checking against *ScS-S* and the shape of the shear wave travel time curve at various stages. Once these data are satisfied, we have an accurate shear velocity profile and a first approximation to the density perturbation. Modes that are sensitive to compressional velocity and density were then inverted for these parameters, with checks being made at various stages of the iterative process against body wave data such as *PcP-P*, *P* wave residuals, and differential core times. The perturbations in density at this stage affected the fits of the toroidal modes, since they are slightly dependent on density. They were consequently reinverted. Modes that are strongly affected by all three parameters were inverted at the end of each iteration cycle in order to decrease the coupling between parameters. More and more higher spheroidal overtones were incorporated into the data set as the number of iterations increased, until it became clear that the fit to the more accurate and complete lower-order data was starting to degrade, while the model itself was almost indistinguishable from earlier iterations. Satisfactory convergence was achieved after about eight iteration cycles and a total of 32 iterations on various subsets of the data. All the modes and body wave parameters were then recomputed. This procedure, although cumbersome, seems preferable to inverting simultaneously for all parameters by using all the normal mode data with equal weight.

THE NORMAL MODE DATA SET

For the first several iterations we used the same 177 modes as used in the study of *Jordan and Anderson* [1974]. This includes the first five radial modes, the fundamental spheroidal modes ${}_0S_2$–${}_0S_{63}$, the fundamental toroidal modes ${}_0T_2$–${}_0T_{46}$, 56 spheroidal overtones, and nine toroidal overtones. Most of these data are from *Dziewonski and Gilbert* [1973] and *Gilbert and Dziewonski* [1975]. *Gilbert and Dziewonski* [1975] have recently presented the results of a new analysis and have tabulated what they feel to be the 'best' observation for each mode. However, their criterion for best is model dependent.

In the final inversions we used 400 representative modes including 148 toroidal overtones up to ${}_7T_{49}$ and 136 spheroidal overtones up to ${}_5S_{35}$. Eight radial modes were used. The data are from *Dziewonski and Gilbert* [1973], *Gilbert and Dziewonski* [1975], *Bolt and Currie* [1975], *Mendiguren* [1973], *Derr* [1969], and H. Kanamori (unpublished results, 1975). Unfortunately, the techniques used by *Mendiguren* [1973] and *Gilbert and Dziewonski* [1975] do not yield reliable estimates of the errors. We follow the latter authors in assuming that 0.05% is a minimum error but otherwise adopt the published error estimates. In many cases the tabulated error is much less than one would infer by comparing the various data sets. The eigenperiods and estimates of their errors are tabulated in Table 2.

For the toroidal data set we have used essentially the same modes as those used by *Gilbert and Dziewonski* [1975] except that we have deleted the data of *Brune and Gilbert* [1974] which have large uncertainties (~0.40%), are not fit well by the Gilbert-Dziewonski models, and represent properties only over a very short arc length of the earth's surface. The remaining data include the fundamental and first seven toroidal overtones having periods greater than 73 s. This process eliminates 156 modes from the Gilbert-Dziewonski toroidal data set.

Although they are not used in the inversion, we have spot-checked modes in each overtone group up to the 22nd spheroidal overtone. Agreement is satisfactory.

RESULTS OF THE INVERSION

The final model, designated C2, fits the toroidal data set, 192 modes, with an average error of 0.09% and the radial-spheroidal data set, 208 modes, with an average error of 0.07%. A

TABLE 1. Summary of Fit of C2 to Normal Mode Data

Modes	Error, %
${}_0S_2$–${}_0S_{29}$	0.03
${}_0S_{30}$–${}_0S_{66}$	0.08
${}_1S_2$–${}_1S_{43}$	0.10
${}_1S_{44}$–${}_1S_{75}$	0.07
${}_2S_3$–${}_2S_{49}$	0.07
${}_2S_{57}$–${}_2S_{76}$	0.15
${}_3S_1$–${}_3S_{54}$	0.05
${}_3S_{58}$–${}_3S_{73}$	0.11
${}_4S_2$–${}_4S_{40}$	0.08
${}_5S_2$–${}_5S_{35}$	0.09
${}_0T_2$–${}_0T_{29}$	0.04
${}_0T_{30}$–${}_0T_{46}$	0.17
${}_0T_{30}$–${}_0T_{46}$	0.08*
${}_1T_2$–${}_1T_{29}$	0.11
${}_1T_{30}$–${}_1T_{66}$	0.07
${}_2T_2$–${}_2T_{61}$	0.08
${}_3T_9$–${}_3T_{72}$	0.08
${}_4T_7$–${}_4T_{66}$	0.16
${}_5T_9$–${}_7T_{49}$	0.09
${}_0S_0$–${}_8S_0$	0.05

Average error for radial-spheroidal data set is 0.07; average error for toroidal data set is 0.09.
*Includes traveling wave data sets.

summary of the fit is given in Table 1. The complete data set along with computed periods for C2 is given in Table 2. The fits to ${}_0S_2$–${}_0S_{29}$ and ${}_0T_2$–${}_0T_{29}$, the fundamental modes, are 0.03% and 0.05%, respectively. These are generally the best-excited and most accurately determined modes, and it is important that they be fit well. More determinations have also been made of these modes, and they therefore represent a better gross earth average than some of the higher modes for which, in many cases, only a single observation is available. Fifty-two of the modes, or 13%, are fit to better than 1 part in 10,000, and 282 modes, or 71%, are fit to 1 part in 1000; 244 modes, or 61%, are fit to 1 standard deviation, and 343, or 86%, are fit to 2 standard deviations. Although this represents a good overall fit, it is not as good as it should be if all the data are independent and if the error estimates are reliable. In spite of the great increase in the normal mode data set there are still some modes whose identification or period assignment is questionable. Of the present 400-mode data set there are 40 modes that are not fit well (>0.15% error) by either C2 or 1066B of

TABLE 2. Observed and Computed Eigenperiods

Mode	Data, s	Error, %	C2	Difference, %
${}_0T_2$	2636.38	0.08	2630.18	0.24
${}_0T_3$	1702.51	0.15	1702.30	0.01
${}_0T_4$	1303.60	0.07	1303.63	0.00
${}_0T_5$	1075.20	0.09	1075.53	−0.03
${}_0T_6$	925.36	0.09	925.55	−0.02
${}_0T_7$	817.92	0.08	818.04	−0.01
${}_0T_8$	736.86	0.05	736.39	0.06
${}_0T_9$	671.80	0.06	671.76	0.01
${}_0T_{10}$	619.02	0.05	619.03	−0.00
${}_0T_{11}$	574.62	0.08	574.99	−0.06
${}_0T_{12}$	536.93	0.05	537.52	−0.11
${}_0T_{13}$	504.94	0.08	505.16	−0.04
${}_0T_{14}$	476.64	0.08	476.86	−0.04
${}_0T_{15}$	451.83	0.06	451.83	−0.00
${}_0T_{16}$	429.50	0.07	429.52	0.00
${}_0T_{17}$	409.61	0.05	409.46	0.04
${}_0T_{18}$	391.16	0.10	391.32	−0.04
${}_0T_{19}$	374.76	0.05	374.80	−0.01
${}_0T_{20}$	359.59	0.08	359.68	−0.03
${}_0T_{21}$	345.70	0.05	345.79	−0.03
${}_0T_{22}$	333.15	0.13	332.97	0.05
${}_0T_{23}$	321.21	0.09	321.10	0.04
${}_0T_{24}$	310.18	0.08	310.06	0.04
${}_0T_{25}$	299.51	0.10	299.78	−0.09
${}_0T_{26}$	290.26	0.06	290.17	0.03
${}_0T_{27}$	281.21	0.16	281.16	0.02
${}_0T_{28}$	272.60	0.27	272.70	−0.04
${}_0T_{29}$	264.66	0.05	264.75	−0.03
${}_0T_{30}$	257.29	0.15	257.25	0.02
${}_0T_{31}$	250.14	0.04	250.16	−0.01
${}_0T_{32}$	243.43	0.07	243.46	0.01
${}_0T_{33}$	237.37	0.10	237.10	0.11
${}_0T_{34}$	231.29	0.10	231.07	0.09
${}_0T_{36}$	219.69	0.11	219.89	−0.09
${}_0T_{37}$	213.89	0.10	214.69	−0.37
${}_0T_{38}$	209.83	0.28	209.73	0.05
${}_0T_{39}$	204.27	0.05	205.00	−0.36
${}_0T_{40}$	199.96	0.19	200.48	−0.26
${}_0T_{41}$	195.88	0.22	196.15	−0.14
${}_0T_{42}$	191.26	0.13	192.00	−0.38
${}_0T_{43}$	187.40	0.26	188.02	−0.32
${}_0T_{44}$	183.78	0.15	184.21	−0.23
${}_0T_{45}$	180.25	0.05	180.54	−0.16
${}_0T_{46}$	176.85	0.05	177.02	−0.09
${}_1T_2$	756.57	0.08	756.22	0.05
${}_1T_3$	695.18	0.07	693.65	0.22
${}_1T_4$	629.98	0.10	629.61	0.06
${}_1T_6$	519.09	0.06	518.53	0.11
${}_1T_7$	475.17	0.13	474.74	0.09
${}_1T_8$	438.49	0.05	438.17	0.07
${}_1T_9$	407.73	0.10	407.57	0.04
${}_1T_{10}$	381.65	0.10	381.68	−0.01
${}_1T_{11}$	359.14	0.05	359.45	−0.09
${}_1T_{12}$	339.54	0.06	340.05	−0.15
${}_1T_{13}$	322.84	0.12	322.91	−0.02
${}_1T_{16}$	280.59	0.06	281.35	−0.27
${}_1T_{20}$	240.98	0.09	241.29	−0.13
${}_1T_{24}$	211.95	0.05	212.22	−0.13
${}_1T_{25}$	205.85	0.05	206.16	−0.15
${}_1T_{26}$	200.27	0.05	200.51	−0.12
${}_1T_{29}$	185.34	0.05	185.57	−0.12
${}_1T_{30}$	180.80	0.06	181.16	−0.20
${}_1T_{31}$	176.85	0.07	177.00	−0.08
${}_1T_{33}$	169.27	0.05	169.32	−0.03
${}_1T_{34}$	165.72	0.05	165.78	−0.04
${}_1T_{35}$	162.36	0.05	162.41	−0.03
${}_1T_{36}$	159.11	0.05	159.20	−0.06
${}_1T_{37}$	156.08	0.05	156.14	−0.04
${}_1T_{38}$	153.17	0.08	153.21	−0.02
${}_1T_{39}$	150.28	0.07	150.41	−0.08
${}_1T_{40}$	147.68	0.05	147.72	−0.03
${}_1T_{41}$	145.12	0.07	145.14	−0.02
${}_1T_{42}$	142.66	0.06	142.67	−0.01
${}_1T_{43}$	140.23	0.08	140.29	−0.04
${}_1T_{44}$	137.96	0.06	138.00	−0.03
${}_1T_{45}$	135.64	0.24	135.79	−0.11
${}_1T_{46}$	133.63	0.07	133.66	−0.02
${}_1T_{47}$	131.59	0.17	131.60	−0.01
${}_1T_{48}$	129.56	0.06	129.62	−0.04
${}_1T_{50}$	125.92	0.08	125.83	0.07
${}_1T_{51}$	124.13	0.43	124.03	0.08
${}_1T_{52}$	122.26	0.14	122.28	−0.02
${}_1T_{54}$	118.96	0.13	118.94	0.02
${}_1T_{57}$	114.41	0.12	114.27	0.12

TABLE 2. (continued)

Mode	Data, s	Error, %	C2	Difference, %
${}_1T_{58}$	112.92	0.12	112.81	0.10
${}_1T_{59}$	111.40	0.09	111.38	0.02
${}_1T_{60}$	110.24	0.13	109.98	0.23
${}_1T_{62}$	107.44	0.13	107.31	0.13
${}_1T_{64}$	104.94	0.13	104.76	0.17
${}_1T_{66}$	102.59	0.14	102.34	0.25
${}_2T_2$	447.30	0.09	448.21	−0.20
${}_2T_4$	419.38	0.09	420.34	−0.23
${}_2T_5$	401.82	0.09	402.63	−0.20
${}_2T_7$	363.65	0.07	363.43	0.06
${}_2T_8$	343.34	0.06	343.43	−0.03
${}_2T_{17}$	219.95	0.06	219.97	−0.01
${}_2T_{18}$	211.90	0.06	212.07	−0.08
${}_2T_{19}$	204.63	0.10	204.83	−0.10
${}_2T_{21}$	191.91	0.06	191.97	−0.03
${}_2T_{22}$	186.19	0.06	186.22	−0.02
${}_2T_{25}$	171.12	0.12	171.14	−0.01
${}_2T_{26}$	166.50	0.07	166.72	−0.13
${}_2T_{27}$	162.58	0.09	162.54	0.02
${}_2T_{28}$	158.43	0.05	158.59	−0.10
${}_2T_{29}$	154.70	0.06	154.85	−0.10
${}_2T_{31}$	147.71	0.06	147.93	−0.15
${}_2T_{32}$	144.59	0.06	144.72	−0.09
${}_2T_{34}$	138.62	0.06	138.74	−0.08
${}_2T_{35}$	135.73	0.06	135.94	−0.16
${}_2T_{36}$	133.14	0.06	133.28	−0.10
${}_2T_{37}$	130.51	0.06	130.72	−0.16
${}_2T_{38}$	128.17	0.08	128.28	−0.09
${}_2T_{39}$	125.71	0.06	125.93	−0.18
${}_2T_{40}$	123.56	0.06	123.68	−0.10
${}_2T_{41}$	121.57	0.05	121.53	0.03
${}_2T_{42}$	119.33	0.14	119.46	−0.11
${}_2T_{44}$	115.49	0.06	115.55	−0.06
${}_2T_{45}$	113.57	0.06	113.72	−0.13
${}_2T_{47}$	110.22	0.06	110.25	−0.02
${}_2T_{49}$	106.98	0.06	107.03	−0.04
${}_2T_{51}$	104.01	0.06	104.03	−0.02
${}_2T_{52}$	102.60	0.06	102.62	−0.02
${}_2T_{54}$	99.93	0.06	99.92	0.01
${}_2T_{55}$	98.61	0.06	98.65	−0.04
${}_2T_{58}$	95.08	0.06	95.04	0.04
${}_2T_{61}$	91.85	0.07	91.76	0.10
${}_3T_9$	259.26	0.12	259.38	−0.05
${}_3T_{11}$	240.50	0.10	240.80	−0.13
${}_3T_{17}$	189.97	0.13	190.77	−0.42
${}_3T_{18}$	184.09	0.09	184.28	−0.10
${}_3T_{19}$	178.17	0.09	178.33	−0.09
${}_3T_{20}$	172.74	0.06	172.87	−0.07
${}_3T_{21}$	167.69	0.06	167.84	−0.09
${}_3T_{23}$	158.54	0.06	158.81	−0.17
${}_3T_{24}$	154.81	0.12	154.72	0.06
${}_3T_{25}$	150.66	0.05	150.87	−0.14
${}_3T_{29}$	137.24	0.07	137.35	−0.08
${}_3T_{33}$	126.16	0.06	126.21	−0.04
${}_3T_{34}$	123.75	0.06	123.72	0.02
${}_3T_{37}$	116.89	0.06	116.87	0.02
${}_3T_{41}$	108.87	0.06	108.94	−0.06
${}_3T_{47}$	99.08	0.06	99.08	0.00
${}_3T_{51}$	93.67	0.09	93.56	0.12
${}_3T_{59}$	84.35	0.09	84.35	0.00
${}_3T_{65}$	78.69	0.10	78.70	−0.01
${}_3T_{72}$	73.16	0.10	73.16	0.00
${}_4T_7$	216.81	0.18	217.27	−0.21
${}_4T_{11}$	199.74	0.19	200.99	−0.17
${}_4T_{14}$	184.86	0.19	185.44	−0.31

TABLE 2. (continued)

Mode	Data, s	Error, %	C2	Difference, %
${}_4T_{16}$	174.72	0.19	175.34	−0.35
${}_4T_{20}$	155.64	0.19	155.80	−0.10
${}_4T_{22}$	147.47	0.19	147.17	0.20
${}_4T_{23}$	143.67	0.19	143.24	0.30
${}_4T_{25}$	136.30	0.20	136.11	0.14
${}_4T_{27}$	130.03	0.23	129.80	0.17
${}_4T_{40}$	101.27	0.30	101.32	−0.05
${}_4T_{45}$	93.79	0.10	93.88	−0.09
${}_4T_{48}$	89.82	0.10	89.98	−0.17
${}_4T_{50}$	87.46	0.09	87.56	−0.12
${}_4T_{54}$	82.95	0.10	83.13	−0.22
${}_4T_{63}$	74.72	0.09	74.68	0.04
${}_4T_{64}$	73.79	0.09	73.86	−0.10
${}_4T_{65}$	72.94	0.10	73.05	−0.15
${}_4T_{66}$	72.28	0.10	72.26	0.03
${}_5T_9$	174.33	0.10	174.67	−0.19
${}_5T_{10}$	171.89	0.08	172.17	−0.16
${}_5T_{15}$	157.57	0.10	157.65	−0.05
${}_5T_{38}$	97.11	0.09	97.11	0.00
${}_5T_{40}$	94.12	0.08	94.12	0.00
${}_5T_{44}$	88.64	0.09	88.69	−0.05
${}_5T_{46}$	87.47	0.09	87.43	0.05
${}_5T_{50}$	81.60	0.10	81.65	−0.06
${}_5T_{55}$	76.52	0.09	76.61	−0.12
${}_5T_{57}$	74.75	0.09	74.78	−0.04
${}_6T_{34}$	97.13	0.10	97.06	0.07
${}_6T_{35}$	95.46	0.09	95.42	0.04
${}_6T_{41}$	86.70	0.09	86.77	−0.09
${}_6T_{42}$	85.35	0.09	85.50	−0.17
${}_6T_{45}$	81.85	0.10	81.90	−0.05
${}_6T_{49}$	77.65	0.09	77.59	0.08
${}_6T_{53}$	73.89	0.09	73.78	0.15
${}_7T_8$	129.67	0.39	129.27	0.31
${}_7T_{17}$	118.57	0.13	118.60	−0.03
${}_7T_{19}$	115.58	0.14	115.69	−0.10
${}_7T_{28}$	101.15	0.13	101.42	−0.26
${}_7T_{29}$	99.53	0.13	99.74	−0.21
${}_7T_{30}$	97.93	0.13	98.05	−0.12
${}_7T_{34}$	91.46	0.14	91.40	0.06
${}_7T_{38}$	85.45	0.13	85.49	−0.05
${}_7T_{40}$	82.84	0.14	82.89	−0.06
${}_7T_{46}$	76.18	0.13	76.19	−0.02
${}_7T_{49}$	73.36	0.15	73.32	0.05
${}_0S_0$	1227.64	0.06	1228.47	−0.07
${}_1S_0$	613.59	0.05	613.91	−0.05
${}_2S_0$	398.55	0.05	398.58	−0.01
${}_3S_0$	305.84	0.05	306.01	−0.05
${}_4S_0$	243.59	0.05	243.44	0.06
${}_5S_0$	204.61	0.05	204.70	−0.05
${}_6S_0$	174.25	0.09	174.10	0.09
${}_8S_0$	134.65	0.05	134.66	0.00
${}_0S_2$	3233.26	0.06	3231.89	0.04
${}_0S_3$	2133.58	0.11	2133.63	0.00
${}_0S_4$	1545.60	0.05	1545.43	0.01
${}_0S_5$	1190.12	0.05	1190.11	0.00
${}_0S_6$	963.17	0.05	963.46	−0.03
${}_0S_7$	811.45	0.05	812.06	−0.08
${}_0S_8$	707.64	0.05	707.68	0.00
${}_0S_9$	633.95	0.05	633.73	0.03
${}_0S_{10}$	580.06	0.05	579.32	0.13
${}_0S_{11}$	536.98	0.05	537.04	−0.01
${}_0S_{12}$	502.33	0.06	502.45	−0.02
${}_0S_{13}$	473.17	0.06	473.27	−0.02
${}_0S_{14}$	448.20	0.05	448.11	0.02
${}_0S_{15}$	426.06	0.05	426.11	−0.01
${}_0S_{16}$	406.75	0.05	406.69	0.01
${}_0S_{17}$	389.32	0.05	389.42	−0.03

TABLE 2. (continued)

Mode	Data, s	Error, %	C2	Difference, %
${}_0S_{18}$	374.02	0.05	373.93	0.02
${}_0S_{19}$	360.11	0.05	359.96	0.04
${}_0S_{20}$	347.50	0.05	347.27	0.07
${}_0S_{21}$	335.81	0.05	335.68	0.04
${}_0S_{22}$	325.06	0.05	325.04	0.01
${}_0S_{23}$	315.21	0.05	315.20	0.00
${}_0S_{24}$	306.25	0.06	306.08	0.06
${}_0S_{25}$	297.66	0.05	297.57	0.03
${}_0S_{26}$	289.60	0.05	289.60	0.00
${}_0S_{27}$	282.18	0.05	282.11	0.02
${}_0S_{28}$	275.11	0.05	275.04	0.03
${}_0S_{29}$	268.44	0.06	268.36	0.03
${}_0S_{30}$	262.06	0.05	262.02	0.02
${}_0S_{31}$	255.95	0.05	256.00	−0.02
${}_0S_{32}$	250.31	0.05	250.26	0.02
${}_0S_{33}$	244.92	0.05	244.78	0.06
${}_0S_{34}$	239.59	0.05	239.53	0.03
${}_0S_{35}$	234.58	0.05	234.52	0.03
${}_0S_{36}$	229.74	0.05	229.70	0.02
${}_0S_{37}$	225.16	0.05	225.08	0.04
${}_0S_{38}$	220.62	0.05	220.64	0.01
${}_0S_{39}$	216.43	0.05	216.37	0.03
${}_0S_{40}$	212.31	0.05	212.25	0.03
${}_0S_{41}$	208.35	0.05	208.28	0.03
${}_0S_{42}$	204.57	0.06	204.46	0.06
${}_0S_{43}$	200.93	0.05	200.76	0.08
${}_0S_{44}$	197.19	0.05	197.19	0.00
${}_0S_{45}$	193.87	0.05	193.74	0.07
${}_0S_{46}$	190.57	0.05	190.40	0.09
${}_0S_{47}$	187.26	0.05	187.17	0.05
${}_0S_{48}$	184.25	0.05	184.05	0.11
${}_0S_{49}$	181.00	0.05	181.02	−0.01
${}_0S_{50}$	178.31	0.05	178.08	0.13
${}_0S_{51}$	175.27	0.05	175.23	0.02
${}_0S_{52}$	172.54	0.05	172.47	0.04
${}_0S_{53}$	169.97	0.05	169.79	0.11
${}_0S_{54}$	167.38	0.05	167.19	0.12
${}_0S_{56}$	162.41	0.09	162.20	0.13
${}_0S_{57}$	160.01	0.05	159.81	0.12
${}_0S_{58}$	157.70	0.09	157.49	0.13
${}_0S_{59}$	155.01	0.05	155.23	0.14
${}_0S_{60}$	153.24	0.05	153.03	0.14
${}_0S_{61}$	151.12	0.05	150.89	0.15
${}_0S_{62}$	149.07	0.05	148.80	0.18
${}_0S_{63}$	147.09	0.05	146.77	0.22
${}_0S_{64}$	144.96	0.09	144.79	0.22
${}_0S_{65}$	142.99	0.09	142.86	0.09
${}_0S_{66}$	141.22	0.09	140.98	0.17
${}_1S_2$	1470.85	0.08	1469.37	0.10
${}_1S_3$	1063.96	0.11	1063.01	0.09
${}_1S_4$	852.67	0.05	851.98	0.08
${}_1S_5$	730.56	0.08	729.59	0.13
${}_1S_6$	657.61	0.05	657.34	0.04
${}_1S_7$	603.93	0.05	604.64	−0.12
${}_1S_8$	556.03	0.07	556.48	−0.08
${}_1S_9$	509.96	0.05	509.97	0.00
${}_1S_{10}$	465.45	0.06	466.18	−0.16
${}_1S_{14}$	337.01	0.05	336.48	0.16
${}_1S_{15}$	316.06	0.05	315.58	0.15
${}_1S_{16}$	299.50	0.09	299.56	−0.02
${}_1S_{17}$	286.22	0.07	286.27	−0.02
${}_1S_{18}$	274.75	0.10	274.45	0.11
${}_1S_{19}$	263.63	0.09	263.72	−0.03
${}_1S_{20}$	253.97	0.09	253.88	0.04
${}_1S_{21}$	244.93	0.09	244.80	0.05
${}_1S_{22}$	236.21	0.09	236.38	−0.07

TABLE 2. (continued)

Mode	Data, s	Error, %	C2	Difference, %
${}_1S_{23}$	228.42	0.09	228.55	−0.06
${}_1S_{24}$	220.99	0.09	221.25	−0.12
${}_1S_{25}$	214.44	0.09	214.43	0.07
${}_1S_{26}$	207.71	0.09	208.03	−0.16
${}_1S_{27}$	201.70	0.09	202.04	−0.17
${}_1S_{28}$	196.31	0.09	196.40	−0.05
${}_1S_{29}$	190.89	0.06	191.10	−0.11
${}_1S_{30}$	185.94	0.09	186.10	−0.09
${}_1S_{32}$	176.71	0.13	176.94	−0.13
${}_1S_{33}$	172.34	0.13	172.73	−0.22
${}_1S_{34}$	168.30	0.13	168.74	−0.26
${}_1S_{35}$	164.60	0.13	164.96	−0.22
${}_1S_{36}$	161.35	0.05	161.38	−0.02
${}_1S_{37}$	157.67	0.13	157.98	−0.19
${}_1S_{38}$	154.76	0.05	157.74	0.01
${}_1S_{39}$	151.64	0.07	151.66	−0.01
${}_1S_{40}$	148.61	0.09	148.72	−0.08
${}_1S_{41}$	145.83	0.05	145.93	−0.07
${}_1S_{42}$	143.17	0.09	143.25	−0.06
${}_1S_{43}$	140.61	0.09	140.69	−0.06
${}_1S_{44}$	138.25	0.09	138.25	0.00
${}_1S_{47}$	131.50	0.13	131.50	0.00
${}_1S_{48}$	129.18	0.13	129.43	−0.19
${}_1S_{49}$	127.14	0.13	127.43	−0.23
${}_1S_{50}$	125.39	0.23	125.51	−0.09
${}_1S_{52}$	121.96	0.05	121.87	0.07
${}_1S_{53}$	120.07	0.05	120.14	−0.06
${}_1S_{54}$	118.50	0.13	118.47	0.03
${}_1S_{55}$	116.81	0.13	116.85	−0.04
${}_1S_{56}$	115.32	0.13	115.29	0.03
${}_1S_{58}$	112.25	0.13	112.30	−0.05
${}_1S_{59}$	110.91	0.13	110.87	0.03
${}_1S_{61}$	108.06	0.13	108.14	−0.07
${}_1S_{63}$	105.69	0.13	105.55	0.13
${}_1S_{64}$	104.41	0.13	104.31	0.10
${}_1S_{68}$	99.71	0.13	99.64	0.07
${}_1S_{75}$	92.48	0.13	92.48	0.00
${}_2S_3$	804.17	0.06	804.95	−0.10
${}_2S_4$	724.87	0.05	725.16	−0.04
${}_2S_5$	660.41	0.05	660.06	0.05
${}_2S_6$	594.71	0.05	594.64	0.01
${}_2S_7$	535.70	0.08	535.80	−0.02
${}_2S_8$	488.01	0.05	487.56	0.09
${}_2S_9$	448.35	0.05	448.27	0.02
${}_2S_{10}$	415.92	0.18	415.81	0.03
${}_2S_{11}$	388.28	0.05	388.49	−0.05
${}_2S_{12}$	365.13	0.05	365.09	0.01
${}_2S_{13}$	344.72	0.06	344.71	0.00
${}_2S_{14}$	326.59	0.09	326.45	0.04
${}_2S_{15}$	309.20	0.05	308.88	0.10
${}_2S_{27}$	174.03	0.06	173.90	0.08
${}_2S_{28}$	169.25	0.05	169.14	0.06
${}_2S_{30}$	160.51	0.05	160.43	0.05
${}_2S_{32}$	152.68	0.24	152.65	0.02
${}_2S_{35}$	142.61	0.05	142.42	0.13
${}_2S_{40}$	128.54	0.05	128.41	0.10
${}_2S_{45}$	117.34	0.06	117.20	0.12
${}_2S_{46}$	115.33	0.06	115.22	0.09
${}_2S_{49}$	108.37	0.26	108.04	0.31
${}_2S_{57}$	98.04	0.26	97.71	0.33
${}_2S_{60}$	94.14	0.26	93.99	0.16
${}_2S_{65}$	88.65	0.26	88.53	0.14
${}_2S_{71}$	82.97	0.26	82.97	0.00
${}_2S_{76}$	78.89	0.26	78.99	−0.13
${}_3S_1$	1058.09	0.08	1058.01	0.01
${}_3S_2$	904.30	0.05	904.32	0.00

TABLE 2. (continued)

Mode	Data, s	Error, %	C2	Difference, %
${}_3S_6$	392.33	0.05	392.00	0.08
${}_3S_7$	372.05	0.05	372.03	0.01
${}_3S_8$	354.56	0.05	354.39	0.05
${}_3S_9$	338.90	0.08	338.53	0.11
${}_3S_{10}$	323.94	0.06	323.92	0.01
${}_3S_{11}$	310.27	0.08	310.19	0.02
${}_3S_{12}$	297.41	0.08	297.22	0.06
${}_3S_{13}$	285.08	0.08	284.93	0.05
${}_3S_{14}$	273.35	0.05	273.29	0.02
${}_3S_{16}$	251.98	0.05	251.98	0.00
${}_3S_{17}$	242.43	0.05	242.29	0.06
${}_3S_{18}$	233.29	0.05	233.23	0.03
${}_3S_{19}$	224.91	0.05	224.76	0.07
${}_3S_{20}$	216.95	0.09	216.84	0.05
${}_3S_{24}$	190.07	0.05	189.94	0.07
${}_3S_{25}$	184.32	0.08	184.20	0.07
${}_3S_{41}$	113.31	0.08	113.23	0.07
${}_3S_{42}$	111.36	0.08	111.24	0.10
${}_3S_{43}$	109.38	0.08	109.34	0.04
${}_3S_{50}$	97.97	0.08	97.79	0.18
${}_3S_{51}$	96.44	0.07	96.36	0.08
${}_3S_{54}$	92.39	0.08	92.34	0.05
${}_3S_{58}$	87.65	0.05	87.55	0.12
${}_3S_{63}$	82.38	0.13	82.30	0.09
${}_3S_{70}$	76.11	0.13	76.05	0.08
${}_3S_{79}$	73.78	0.13	73.68	0.14
${}_4S_2$	580.81	0.10	580.67	0.02
${}_4S_3$	489.05	0.07	488.23	0.17
${}_4S_4$	439.17	0.11	438.48	0.16
${}_4S_5$	414.62	0.06	414.50	0.03
${}_4S_9$	269.59	0.06	269.86	−0.10
${}_4S_{10}$	258.85	0.08	259.01	−0.06
${}_4S_{11}$	249.60	0.08	249.59	0.00
${}_4S_{12}$	240.78	0.06	241.00	−0.09
${}_4S_{13}$	232.75	0.06	233.00	−0.11
${}_4S_{14}$	225.08	0.06	225.41	−0.15
${}_4S_{15}$	218.17	0.05	218.17	0.00
${}_4S_{20}$	186.33	0.06	186.17	0.08
${}_4S_{40}$	115.44	0.06	115.29	0.13
${}_5S_2$	479.34	0.05	477.86	0.31
${}_5S_3$	460.78	0.05	460.63	0.03
${}_5S_4$	420.36	0.05	420.42	−0.01
${}_5S_5$	370.10	0.05	370.06	0.01
${}_5S_6$	332.11	0.05	332.29	−0.05
${}_5S_7$	303.98	0.05	304.04	−0.02
${}_5S_8$	283.56	0.05	283.82	−0.09
${}_5S_{10}$	237.81	0.05	238.02	−0.09
${}_5S_{12}$	213.03	0.05	213.57	−0.25
${}_5S_{15}$	187.75	0.05	188.07	−0.17
${}_5S_{16}$	181.74	0.06	181.92	−0.10
${}_5S_{20}$	162.45	0.06	162.51	−0.04
${}_5S_{25}$	143.59	0.05	143.52	0.05
${}_5S_{30}$	128.51	0.06	128.52	−0.01
${}_5S_{35}$	116.63	0.06	116.56	0.06
${}_6S_1$*	505.81	0.05	504.46	0.27
${}_6S_{15}$	178.76	0.09	178.59	0.10
${}_6S_{28}$	123.51	0.06	123.60	−0.07
${}_6S_{39}$	100.68	0.09	100.54	0.14
${}_7S_2$	397.37	0.05	397.07	0.08
${}_7S_4$	293.20	0.05	292.98	0.08
${}_7S_{10}$	209.42	0.13	209.74	−0.15
${}_7S_{25}$	125.48	0.09	125.79	−0.19
${}_7S_{35}$	101.74	0.09	102.01	−0.26
${}_8S_1$	348.12	0.05	347.67	0.13
${}_8S_5$	239.96	0.05	240.20	−0.10
${}_8S_{30}$	106.04	0.09	105.97	0.07
${}_9S_2$	310.04	0.09	309.27	0.25

TABLE 2. (continued)

Mode	Data, s	Error, %	C2	Difference, %
${}_{10}S_2$	247.74	0.05	246.80	0.38
${}_{10}S_{16}$	134.95	0.05	134.88	0.05
${}_{11}S_1$	271.36	0.09	271.47	−0.04
${}_{11}S_{24}$	104.43	0.05	104.63	−0.19
${}_{12}S_7$	170.69	0.05	171.02	−0.19
${}_{13}S_1$	222.69	0.09	222.82	−0.06
${}_{13}S_{19}$	103.43	0.06	103.52	−0.09
${}_{14}S_4$	180.81	0.13	180.43	0.20
${}_{15}S_3$	165.83	0.05	165.63	0.12
${}_{15}S_{16}$	100.77	0.05	100.90	−0.13
${}_{16}S_2$	175.29	0.05	175.81	−0.30
${}_{16}S_{10}$	118.62	0.09	118.58	0.03
${}_{17}S_{18}$	100.48	0.09	100.43	0.05
${}_{18}S_3$	145.28	0.05	145.27	0.00
${}_{18}S_8$	115.62	0.05	116.04	−0.36
${}_{19}S_9$	110.55	0.05	110.41	0.13
${}_{19}S_{11}$	103.63	0.09	103.49	0.14
${}_{20}S_4$	123.18	0.05	123.15	0.02
${}_{20}S_9$	102.09	0.06	101.98	0.11
${}_{21}S_6$	112.96	0.05	112.93	0.03
${}_{21}S_8$	105.36	0.05	105.18	0.17
${}_{22}S_1$	127.88	0.09	127.80	0.06

*From this point on, the modes were spot checks and were not used in the inversion.

Dziewonski and Gilbert [1973] and are inconsistent with adjacent modes. When these modes are deleted, C2 satisfies 68% of the data to 1 standard deviation and 95% of the data to 2 standard deviations. Model C2 is therefore a statistically satisfactory fit to the normal mode data set. The fit to the short-period fundamental mode data, ${}_0T_{37}$–${}_0T_{45}$, is improved when surface wave data are incorporated into the data set.

TABLE 3. Fit of C2 to Short-Period Toroidal and Love Wave Dispersion Data

Mode	Observations*	Error, %	C2	C2 Difference, %	1066B†	1066B Difference, %
${}_0T_{21}$	345.60	0.15	345.79	−0.05	346.02	−0.12
${}_0T_{22}$	332.75	0.13	332.97	−0.07	333.21	−0.14
${}_0T_{23}$	320.92	0.12	321.10	−0.06	321.35	−0.14
${}_0T_{24}$	310.00	0.14	310.06	−0.02	310.32	−0.10
${}_0T_{25}$	299.81	0.16	299.78	0.01	300.05	−0.08
${}_0T_{26}$	290.12	0.15	290.17	−0.02	290.45	−0.11
${}_0T_{27}$	281.16	0.15	281.16	0.00	281.45	−0.10
${}_0T_{28}$	272.70	0.15	272.70	0.00	273.00	−0.11
${}_0T_{29}$	264.72	0.14	264.75	−0.01	265.05	−0.12
${}_0T_{30}$	257.19	0.14	257.25	−0.02	257.56	−0.14
${}_0T_{31}$	250.13	0.14	250.16	−0.01	250.47	−0.14
${}_0T_{32}$	243.65	0.23	243.46	0.08	243.78	−0.05
${}_0T_{33}$	237.11	0.16	237.10	0.00	237.43	−0.14
${}_0T_{34}$	231.06	0.17	231.07	−0.00	231.40	−0.15
${}_0T_{36}$	220.07	0.26	219.89	0.08	220.22	−0.07
${}_0T_{37}$	214.33	0.22	214.69	−0.17	215.03	−0.33
${}_0T_{38}$	209.68	0.17	209.73	−0.02	210.07	−0.19
${}_0T_{39}$	204.65	0.17	205.00	−0.17	205.34	−0.38
${}_0T_{40}$	200.19	0.17	200.48	−0.15	200.82	−0.32
${}_0T_{41}$	195.94	0.14	196.15	−0.11	196.49	−0.28
${}_0T_{42}$	191.65	0.19	192.00	−0.18	192.34	−0.36
${}_0T_{43}$	187.73	0.19	188.02	−0.15	188.36	−0.34
${}_0T_{44}$	183.99	0.17	184.21	−0.12	184.55	−0.30
${}_0T_{45}$	180.38	0.15	180.54	−0.09	180.88	−0.28
${}_0T_{46}$	176.91	0.15	177.02	−0.06	177.36	−0.25

*Average of *Kanamori* [1970], *Dziewonski et al.* [1972], and *Gilbert and Dziewonski* [1975].

†*Gilbert and Dziewonski* [1975].

TABLE 4. Group Velocities

Mode	T, s		U, km/s	
	DMB	C2	DMB	C2
${}_0S_{10}$	579.40	579.32	5.67	5.66
${}_0S_{12}$	502.43	502.45	5.01	5.01
${}_0S_{15}$	426.12	426.11	4.54	4.55
${}_0S_{21}$	335.93	335.68	3.93	3.94
${}_0S_{25}$	297.78	297.57	3.73	3.72
${}_0S_{29}$	268.48	268.36	3.62	3.62
${}_0S_{35}$	234.58	234.52	3.57	3.58
${}_0S_{40}$	212.34	212.25	3.58	3.59
${}_0S_{45}$	193.88	193.74	3.60	3.62
${}_0T_{10}$	617.47	619.03	5.07	5.01
${}_0T_{13}$	503.38	505.16	4.76	4.74
${}_0T_{16}$	428.14	429.52	4.58	4.58
${}_0T_{21}$	344.90	345.79	4.46	4.46
${}_0T_{25}$	299.12	299.78	4.43	4.43
${}_0T_{29}$	264.19	264.75	4.42	4.41
${}_0T_{41}$	195.68	196.15	4.42	4.41
${}_0T_{46}$	176.62	177.02	4.42	4.41

DMB denotes *Dziewonski et al.* [1972].

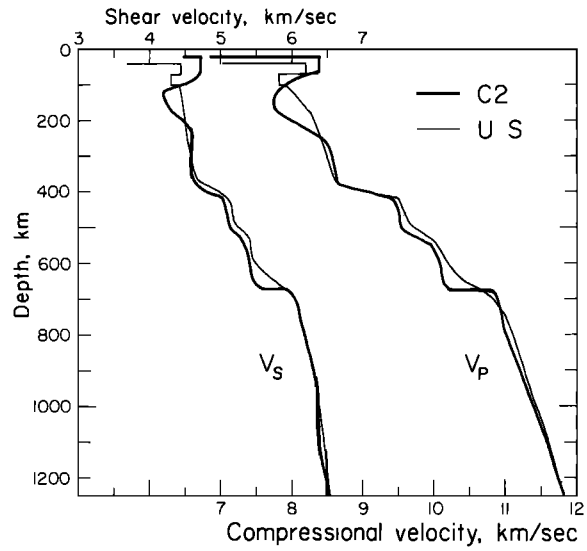

Fig. 2. Upper mantle structure of C2 compared with results of *Helmberger and Wiggins* [1971] and *Helmberger and Engen* [1974] which are based on amplitude and wave form studies in the western United States.

There is considerable spread in measured values for the shorter-period fundamental toroidal oscillations. This probably represents real lateral variations in the structure of the upper mantle. *Kanamori* [1970] and *Dziewonski et al.* [1972] have measured the dispersion of Love waves over a considerable number of great circle paths. These data can be used to augment the data of *Gilbert and Dziewonski* [1975] in order to obtain a more representative gross earth data set. Table 3 gives the values obtained for ${}_0T_{21}-{}_0T_{46}$ by averaging the above data sets with equal weight. The error is the standard deviation of the data groups and does not include the errors associated with the individual groups. Table 2 also gives some spot checks of the very high spheroidal overtone data (37 modes). These additional modes were not used in the inversion, but the fit is comparable to that of the models of *Gilbert and Dziewonski* [1975].

C2 group velocities are compared with the results of *Dziewonski et al.* [1972] in Table 4. The data set is not so large or representative in this case, but the agreement is good.

Although the number of modes inverted is considerably less than the 1066 considered by *Gilbert and Dziewonski* [1975], they constitute a representative data set, particularly when one considers that the total data set includes only 57 significant earth data [*Backus and Gilbert*, 1968; *Gilbert et al.*, 1973; *Gilbert and Dziewonski*, 1975]. Many of the additional modes do not contain information independent of that contained in the differential travel times and the modes considered in this paper. The additional modes also do not contribute substantially to the resolving power required to distinguish between models of the upper mantle. For example, compare the upper mantles of 1066A and 1066B in *Gilbert and Dziewonski* [1975]. The former used a smooth upper mantle as a starting

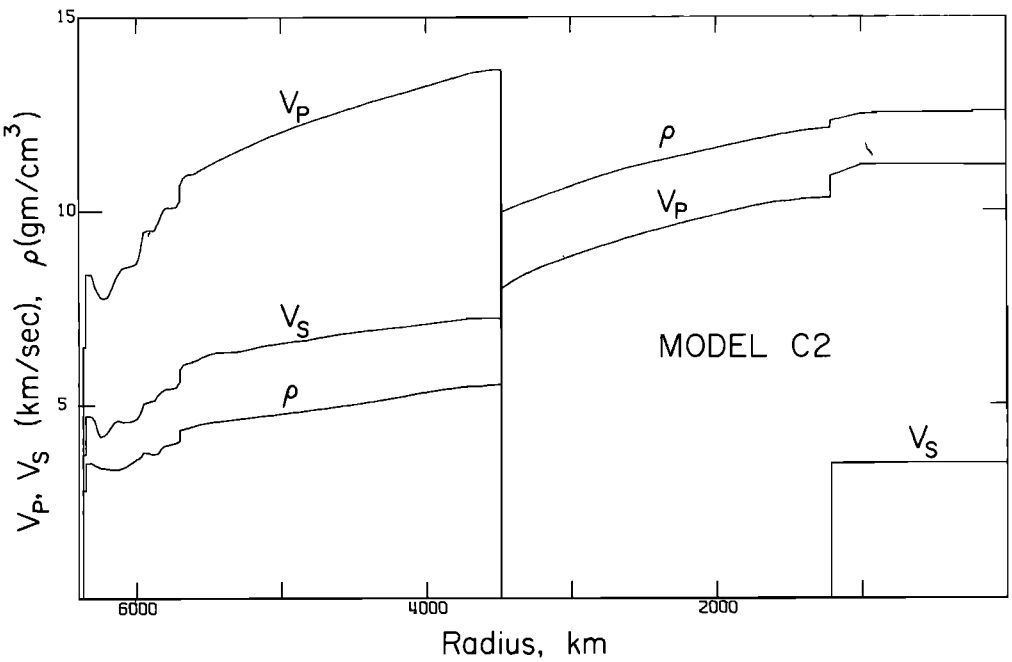

Fig. 1. Model C2. V_p (compressional velocity), V_s (shear velocity), and ρ (density) as a function of radius.

TABLE 5. Model C2: Velocities, Density, Elastic Constants, Pressure, and Gravity as a Function of Radius and Depth

INDEX	RADIUS (KM)	DEPTH (KM)	VP (KM/S)	VS (KM/S)	RHO (G/CM**3)	PHI (KM/S)**2	K (KB)	MU (KB)	LAMBDA (KB)	SIGMA	PRESSURE (KB)	G (CM/S**2)
1	1	6370	11.17	3.50	12.58	108.44	13636	1540	12609	0.4456	3617	0
2	100	6271	11.18	3.50	12.57	108.56	13650	1541	12623	0.4456	3614	52
3	300	6071	11.19	3.50	12.53	108.85	13641	1536	12617	0.4457	3592	122
4	400	5971	11.20	3.50	12.53	109.00	13654	1533	12632	0.4459	3575	150
5	600	5771	11.20	3.50	12.52	109.10	13660	1530	12640	0.4460	3529	218
6	800	5571	11.20	3.48	12.52	109.27	13680	1519	12667	0.4464	3466	286
7	1000	5371	11.17	3.47	12.48	108.81	13579	1502	12578	0.4467	3385	355
8	1215	5156	10.89	3.46	12.30	102.60	12624	1470	11644	0.4439	3281	427
9	1215	5156	10.33	0.0	12.12	106.75	12939	0	12939	0.5000	3281	427
10	1300	5071	10.31	0.0	12.09	106.38	12866	0	12866	0.5000	3236	454
11	1400	4971	10.28	0.0	12.05	105.75	12742	0	12742	0.5000	3179	486
12	1500	4871	10.24	0.0	11.99	104.89	12577	0	12577	0.5000	3116	517
13	1600	4771	10.21	0.0	11.92	104.20	12425	0	12425	0.5000	3055	549
14	1700	4671	10.14	0.0	11.85	102.90	12192	0	12192	0.5000	2988	580
15	1800	4571	10.06	0.0	11.77	101.19	11909	0	11909	0.5000	2917	611
16	1900	4471	9.98	0.0	11.69	99.51	11628	0	11628	0.5000	2844	641
17	2100	4271	9.79	0.0	11.52	95.82	11040	0	11040	0.5000	2688	702
18	2200	4171	9.71	0.0	11.44	94.24	10781	0	10781	0.5000	2606	731
19	2300	4071	9.61	0.0	11.36	92.30	10484	0	10484	0.5000	2520	760
20	2400	3971	9.51	0.0	11.28	90.38	10193	0	10193	0.5000	2433	789
21	2500	3871	9.41	0.0	11.20	88.46	9903	0	9903	0.5000	2342	818
22	2600	3771	9.30	0.0	11.10	86.53	9607	0	9607	0.5000	2249	846
23	2700	3671	9.19	0.0	11.00	84.38	9283	0	9283	0.5000	2154	874
24	2800	3571	9.07	0.0	10.89	82.23	8952	0	8952	0.5000	2057	901
25	2900	3471	8.95	0.0	10.76	80.12	8623	0	8623	0.5000	1958	928
26	3000	3371	8.82	0.0	10.63	77.75	8266	0	8266	0.5000	1858	953
27	3200	3171	8.55	0.0	10.37	73.11	7577	0	7577	0.5000	1652	1003
28	3300	3071	8.39	0.0	10.23	70.40	7202	0	7202	0.5000	1548	1027
29	3400	2971	8.18	0.0	10.09	66.96	6756	0	6756	0.5000	1442	1050
30	3485	2886	7.98	0.0	9.96	63.74	6349	0	6349	0.5000	1352	1069
31	3485	2886	13.64	7.23	5.53	116.38	6431	2885	4508	0.3049	1352	1069
32	3510	2861	13.63	7.24	5.50	115.99	6382	2884	4459	0.3036	1337	1065
33	3550	2821	13.62	7.23	5.50	115.82	6366	2876	4449	0.3037	1314	1060
34	3625	2746	13.59	7.22	5.47	115.07	6299	2857	4394	0.3030	1270	1050
35	3700	2671	13.53	7.21	5.45	113.85	6208	2836	4318	0.3018	1227	1042
36	3775	2596	13.45	7.18	5.43	112.27	6096	2799	4230	0.3009	1185	1034
37	3850	2521	13.37	7.14	5.40	110.64	5973	2755	4136	0.3001	1143	1028
38	3925	2446	13.28	7.11	5.36	109.01	5841	2711	4034	0.2990	1102	1022
39	4000	2371	13.20	7.07	5.31	107.56	5713	2659	3941	0.2986	1061	1017
40	4075	2296	13.12	7.04	5.27	106.09	5589	2611	3848	0.2979	1021	1012

41	4150	2221	13.04	7.01	5.22	104.63	5457	2561	3750	0.2971	981	1008
42	4225	2146	12.97	6.98	5.16	103.20	5329	2515	3653	0.2961	942	1005
43	4300	2071	12.89	6.95	5.12	101.73	5204	2470	3557	0.2951	903	1002
44	4375	1996	12.80	6.92	5.07	100.13	5078	2427	3460	0.2939	865	999
45	4450	1921	12.71	6.89	5.03	98.42	4951	2386	3361	0.2924	827	997
46	4525	1846	12.63	6.85	4.99	96.86	4836	2343	3274	0.2914	789	995
47	4600	1771	12.54	6.81	4.96	95.27	4722	2301	3188	0.2904	752	994
48	4675	1696	12.44	6.77	4.92	93.76	4612	2253	3110	0.2899	715	993
49	4750	1621	12.36	6.72	4.88	92.51	4514	2203	3046	0.2902	679	992
50	4825	1546	12.26	6.67	4.84	91.12	4412	2152	2977	0.2902	643	992
51	4900	1471	12.16	6.63	4.81	89.33	4292	2112	2884	0.2886	607	991
52	4975	1396	12.06	6.59	4.77	87.41	4170	2075	2787	0.2866	571	991
53	5050	1321	11.95	6.56	4.74	85.43	4047	2038	2688	0.2844	536	991
54	5125	1246	11.83	6.52	4.71	83.35	3922	1998	2590	0.2823	501	992
55	5200	1171	11.71	6.45	4.67	81.52	3809	1945	2513	0.2819	466	992
56	5275	1096	11.58	6.38	4.64	79.67	3697	1890	2437	0.2816	431	993
57	5350	1021	11.45	6.37	4.61	76.98	3546	1867	2302	0.2761	397	994
58	5425	946	11.31	6.36	4.58	74.06	3389	1849	2156	0.2691	362	995
59	5500	871	11.17	6.31	4.54	71.78	3258	1805	2055	0.2662	328	997
60	5550	821	11.07	6.23	4.51	70.83	3194	1750	2027	0.2683	306	998
61	5573	798	11.03	6.17	4.50	70.86	3185	1710	2045	0.2723	295	998
62	5602	769	10.96	6.13	4.46	69.96	3119	1674	2003	0.2723	282	999
63	5625	746	10.95	6.09	4.43	70.40	3115	1640	2022	0.2761	272	999
64	5643	728	10.95	6.08	4.41	70.56	3111	1629	2025	0.2771	264	999
65	5660	711	10.91	6.06	4.40	69.99	3079	1614	2003	0.2769	257	1000
66	5675	696	10.86	6.04	4.38	69.44	3040	1595	1976	0.2766	250	1000
67	5700	671	10.64	5.90	4.36	66.92	2915	1516	1905	0.2785	239	1000
68	5700	671	10.25	5.60	4.07	63.18	2571	1277	1720	0.2869	239	1000
69	5725	646	10.11	5.45	4.03	62.62	2520	1195	1724	0.2953	229	1000
70	5750	621	10.09	5.43	4.00	62.44	2499	1182	1711	0.2957	219	1000
71	5775	596	10.08	5.42	3.98	62.47	2484	1168	1706	0.2969	209	999
72	5800	571	10.07	5.40	3.95	62.55	2472	1154	1703	0.2980	199	999
73	5825	546	9.93	5.34	3.90	60.53	2359	1113	1617	0.2962	189	999
74	5850	521	9.70	5.26	3.76	57.10	2143	1040	1450	0.2912	180	998
75	5875	496	9.51	5.12	3.74	55.40	2071	980	1418	0.2956	170	997
76	5900	471	9.51	5.10	3.76	55.76	2096	976	1444	0.2981	161	997
77	5925	446	9.50	5.07	3.79	55.99	2123	976	1472	0.3006	152	996
78	5950	421	9.46	5.04	3.80	55.60	2110	965	1467	0.3016	142	996
79	5967	404	9.12	4.86	3.69	51.79	1909	870	1329	0.3022	136	995
80	5983	388	8.79	4.71	3.62	47.68	1726	802	1192	0.2990	130	995

TABLE 5. (continued)

INDEX	RADIUS (KM)	DEPTH (KM)	VP (KM/S)	VS (KM/S)	RHO (G/CM**3)	PHI (KM/S)**2	K (KB)	MU (KB)	LAMBDA (KB)	SIGMA	PRESSURE (KB)	G (CM/S**2)
81	6000	371	8.64	4.64	3.59	46.01	1653	773	1138	0.2977	124	994
82	6025	346	8.60	4.59	3.53	45.80	1617	744	1121	0.3005	115	994
83	6050	321	8.58	4.57	3.47	45.70	1584	725	1101	0.3015	106	993
84	6075	296	8.55	4.57	3.41	45.31	1544	712	1070	0.3002	98	992
85	6100	271	8.52	4.59	3.37	44.62	1503	709	1031	0.2963	89	991
86	6125	246	8.40	4.62	3.34	42.06	1406	713	931	0.2831	81	990
87	6150	221	8.19	4.57	3.34	39.30	1313	697	849	0.2746	73	989
88	6175	196	7.98	4.45	3.35	37.26	1249	663	807	0.2746	64	988
89	6200	171	7.78	4.30	3.37	35.90	1209	623	794	0.2801	56	987
90	6225	146	7.75	4.22	3.39	36.35	1229	602	828	0.2894	48	986
91	6250	121	7.79	4.18	3.40	37.29	1267	594	871	0.2972	39	985
92	6270	101	7.93	4.36	3.44	37.64	1292	652	858	0.2841	33	984
93	6290	81	8.08	4.62	3.46	36.83	1280	742	785	0.2569	26	984
94	6310	61	8.38	4.72	3.52	40.47	1424	733	902	0.2676	19	984
95	6330	41	8.38	4.73	3.51	40.31	1412	785	889	0.2656	12	983
96	6350	21	8.38	4.71	3.49	40.62	1418	775	902	0.2690	5	983
97	6350	21	6.50	3.72	2.80	23.79	665	387	407	0.2564	5	983
98	6368	3	6.50	3.72	2.80	23.79	665	387	407	0.2563	3	982
99	6368	3	1.45	0.0	1.02	2.10	21	0	21	0.5000	3	982
100	6371	0	1.45	0.0	1.02	2.10	21	0	21	0.5000	0	981

model, and the latter used B1, a model with two upper mantle discontinuities, as a starting model. The smooth starting model remained smooth, showing that the additional modes cannot resolve the detail which is apparent from body wave studies. Additionally, when B1 was subjected to reinversion with the use of all 1066 modes, there were very few changes required, usually amounting to less than 0.05%, and the changes introduced in the upper mantle were in the same direction and generally of the same nature as the differences between C2 and B1. We feel therefore that our procedure of using high-resolution body wave structures as starting models in the inversion and checking the resulting model against both the very high overtone data and the body wave data is at least equivalent to, and perhaps better than, a procedure that relies exclusively on the short-period higher-mode data. The fact that the lower mantle and core of C2 are very similar to those of the Gilbert-Dziewonski models, which were based on all 1066 modes, justifies this approach.

THE RESULTING MODEL

The inverted model, C2, is shown in Figures 1 and 2. The model parameters are given in Table 5. In addition to V_p, V_s, and density as a function of layer index, radius, and depth we also tabulate the seismic parameter $\Phi(= K/\rho = V_p^2 - (4/3)V_s^2)$, bulk modulus K, rigidity μ, Lamé constant λ, Poisson's ratio σ, pressure, and gravity. Also shown in Figure 2 are the Helmberger-Wiggins-Engen profiles, which can be considered models of the upper mantle under western North America. Except for the large differences in the structure of the low-velocity zone and the lithospheric lid the main effect of the inversion was to decrease both P and S velocities between the 400- and 670-km discontinuities by about 0.05–0.1 km/s.

The average lithospheric velocities of C2 are 8.38 and 4.71 km/s for V_p and V_s, respectively. These can be compared with 8.28 ± 0.03 and 4.79 ± 0.04 km/s recorded over long distances in the Pacific [*Sutton and Walker*, 1972] and 8.27 ± 0.01 and 4.75 ± 0.07 km/s for P_n and S_n over the Australian shield [*Simpson*, 1973]. *Hart and Press* [1973] determined a value of 4.71 km/s for S_n for 50- to 150-m.y.-old oceanic lithosphere. There is evidence from refraction studies that V_p may be as high as 8.6 km/s in the lower lithosphere [e.g., *Kosminskaya et al.*, 1972]. These studies are consistent with the average velocities of the lithosphere found here. The depth to the top of the low-velocity zone is 61 km, although this could be increased to about 80 km if the entry into the low-velocity zone is abrupt rather than gradual. The thickness of the LVZ is about 180 km. The density of the uppermost mantle is 3.50 g/cm³ (see, however, the discussion on resolving power below). A small amount of structure in the shear velocity is evident between about 670- and 1200-km depth. This results in a pronounced dip in the S wave residual near 40°, as required by the studies of *Ibrahim and Nuttli* [1967] and *Hart* [1975]. The shape of the S wave residual curve beyond 60° for C2 is also more in line with body wave studies [i.e., *Hales and Roberts*, 1970] than is that for B1.

The major effect of the inversion on core velocities is an increase of about 0.05 km/s from the starting model. The other effects of the inversion are slight changes in the velocity gradient in the outer 400 km of the core, an increase in the velocity gradient in the outer part of the inner core, and a decrease in the velocity jump across the outer core–inner core boundary. The density jump and compressional velocity jump at the boundary are, 0.02 g/cm³ and 0.56 km/s, respectively. The average density, compressional velocity, and shear velocity of the inner core are 12.52 g/cm³, 11.19 km/s, and 3.50

km/s. The shear velocity at the top of the inner core is 3.46 km/s.

The small compressional velocity jump at the inner core–outer core boundary (+0.56 km/s) is in agreement with the evidence from amplitudes of long-period core phases [*Müller*, 1973] which gives 0.58 km/s. The high velocity gradient at the top of the inner core is also consistent with amplitude studies [*Müller*, 1973]. The shear velocity at the top of the inner core, 3.46 km/s, is in general agreement with the bounds, 3–4 km/s, established by *Müller* [1973].

There is some evidence for inhomogeneity in the outer core, at both its upper and its lower boundaries. The velocity gradient is about 0.24 km/s per 100 km at the top of the core decreasing to 0.13 km/s at a radius of 2800 km or about 700 km deep into the core. The gradient then decreases gradually to 0.08 km/s per 100 km at a radius of 1700 km. The velocity increases much more slowly, 0.03 km/s per 100 km in the lowermost 500 km of the outer core. A similar effect occurs in the density profile, with a relatively high density gradient in the outer portion of the core compared with that at deeper levels.

It is of interest to compare the lower mantle and core of C2 with 1066A and 1066B [*Gilbert and Dziewonski*, 1975]. *Gilbert and Dziewonski* [1975] utilized the complete high-overtone data set, while we leaned more heavily on the nominally equivalent body waves and the more abundant fundamental and lower-overtone data and only utilized a sparse sampling of the high-overtone data. Below a radius of 5600 km the mantle shear velocities and densities for these models are virtually identical. The *P* velocities differ at most by 0.2 km/s; the main difference is that the *P* velocity for the 1066 models has a long wavelength oscillation, while that of the C2 is much smoother. *Dziewonski et al.* [1975], using the full mode data set, also have a smooth lower mantle for V_p. The density and V_p in the core are also in very good agreement. There are small differences in the inner core for V_p and V_s. In C2 the slight structure for V_p in the inner core, particularly the rapid increase in the outer portion, is inherited from the starting model of *Whitcomb* [1973] and is therefore a requirement of the core phases rather than of the modes. The differences between C2, 1066A, and 1066B in the inner core are probably unresolvable by using the modes alone. The differences are slight. For example, V_p at the top of the inner core ranges from 10.97 km/s (1066A), 11.04 km/s (1066B), and 10.89 km/s (C2), a spread of 1%. The central V_p is 11.34 km/s (1066A), 11.28 km/s (1066B), and 11.17 km/s (C2), also a spread of 1%. The average V_s for the inner core is 3.57 km/s (1066A), 3.50 km/s (1066B), and 3.48 km/s (C2). The major difference among the models is the density of the inner core. This is not unexpected, since the resolving power for density is very poor in this region. This is unfortunate, since the density is the main constraint on the composition of the inner core. If the density jump at the outer core–inner core boundary is small, as in C2, then the inner core can be the same material as the outer core, since freezing at core pressures can be expected to increase the density only slightly. If the density jump is large, then it is probable that the inner core is lacking in the light elements that are required to satisfy the outer core densities. Average inner core densities are 13.12 g/cm^3 (1066A), 12.85 g/cm^3 (1066B), and 12.35 g/cm^3 (C2). The density of iron at inner core pressures is about 12.9–13.4 g/cm^3.

Resolution

The resolving power of gross earth data has been discussed by *Backus and Gilbert* [1968] and *Jordan and Anderson* [1974]. Although the data set used in the present inversion is more extensive than that used by the latter authors, we use their estimates of averaging lengths as conservative guides. The trade-offs between parameters such as density and shear velocity are also discussed by *Jordan and Anderson* [1974], and *Dziewonski* [1971]. These trade-offs make it particularly important to have independent estimates of the shear velocity structure and to fit first those modes that are sensitive to shear velocity.

Resolution is poor for density below 2400 km, shear velocity structure in the inner core and in the lower 500 km of the mantle, and compressional velocity in the vicinity of 2400-km radius. In these regions, only very long wavelength perturbations from the starting model are justified by the data. The averaging lengths for shear velocity in the upper mantle and transition region are about 200 and 400 km, respectively. The averaging kernels for V_p in the outer core are about 1000 km. As *Jordan and Anderson* [1974] point out, the density of the lithosphere cannot be discussed with any useful precision because the averaging length for density in the upper mantle is about 400 km. However, the high average shear velocity in the lithosphere is resolvable and is consistent with body wave data. Structure in the lithosphere is not resolvable. The averaging lengths for density in the lower mantle are about 1000 km.

Considering the above facts, the slight reversals in shear velocity below 246-km (0.05 km/s over 100 km) depth and in density below 421-km (0.06 g/cm^3 over 25 km) depth are clearly not resolvable.

Compressional Waves

Most recent studies indicate that the JB tables for *P* waves are slow by up to 3 s. Qualitatively, the present study indicates the same thing, but the average discrepancy between 30° and 95° is only 1.2 s with maximum deviations from JB times near 30° (1.6 s) and between 55° and 75° (1.7–3.0 s). Model C2 is 1.5 s slow, on the average, over the range 30°–95°, in comparison with the 1968 tables, with the residuals decreasing from 2.4 s at 30° to 0.8 s at 80° and increasing to 1.5 s at 95°. A possible bias of this type in the 1968 tables was pointed out by *Jordan and Anderson* [1974]. The travel times of *Hales et al.* [1968] agree with those predicted by C2 to within 0.6 s with maximum deviations of 1 s at 45° and 90°. Model C2 averages 0.6 slower than the data of *Hales et al.* [1968]. The discrepancies between the various body wave studies confound efforts to determine differences between the 'average' mantle (free oscillations) and tectonic to continental paths (most body wave studies), but the present study combined with the most recent body wave data suggests that the average earth is about 0.6 s slower than that portion of the earth available to study by body wave techniques, i.e., continental sources and receivers. Alternatively, one could say that C2 is consistent with *P* wave travel time studies, since it falls between the JB and the 1968 solutions [*Herrin et al.*, 1968] and is close to solutions of *Cleary and Hales* [1966], *Hales et al.* [1968], and *Carder et al.* [1966]. Throughout most of the distance range between 30° and 95°, C2 is slightly slower than the three 1966 studies and is closest to *Cleary and Hales* [1966]; see Figure 3 and Table 6.

Table 7 compares the apparent velocities ($dt/d\Delta$) of C2 with four sets of published data. The fit is satisfactory in that predicted values fall within the scatter of the observations except near 85°, but even there the difference is only 0.6%.

Model C2 averages 2 s faster than JB times for *PcP* between 30° and 90° (Table 8). The difference in the size of the core accounts for about 1.8 s of this difference. The remainder is accounted for by the 0.3-s difference in travel times between JB

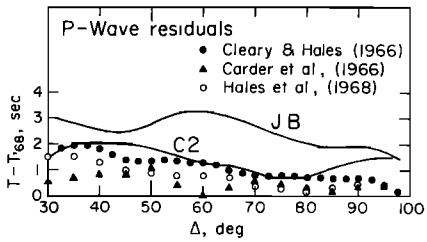

Fig. 3. Compressional velocity residuals, relative to the 1968 tables [*Herrin et al.*, 1968], of C2 and other recent studies. Jeffreys-Bullen (JB) times are also shown.

and C2 at 95°. *PcP* times from Pacific events [*Gogna*, 1973] agree with C2 to 0.3 s, ranging from +2.2 s at 50° to −2.0 s at 80° (observed minus computed values). The modified *PcP* times [*Engdahl and Johnson*, 1974] consistent with the 1968 tables average 1.3 s faster than model C2. Since these times were determined from differential *PcP-P* times and the B1, and C2, core radius, this difference must be accounted for in mantle velocities. In fact, the 1968 tables average 1.5 s faster than C2 for *P* waves between 30° and 95°. Within the uncertainty of the data, no statement can be made from *PcP* data regarding the differences between the average earth and the body wave solutions. The C2 *PcP-P* times (Table 9) average 0.5 s fast between 30° and 60° and 0.3 s slow beyond 65° but seem to be generally consistent with the data.

The core phase *PKP* averages 1.7 s faster for C2 than for JB. This is in agreement, within 0.3 s, with the differences in *PcP* times and therefore can be accounted for by differences in core radii and mantle velocities. The differential core times ($P_{AB}' - P_{DF}'$, $P_{BC}' - P_{DF}'$) agree with the recent study of *Whitcomb* [1973], with differences ranging from +0.4 to −0.9 s. For comparison, other *PKP* data are tabulated in Table 10. The average difference between C2 and the 1968 tables is −0.3 s. The *PKP* times for the AB and BC branches for C2 are generally bracketed by the values given in the 1968 tables and the times given by *Whitcomb* [1973]. However, the DF branch is generally 1–2 s fast. This could be corrected (1) by decreasing the velocity of the region surrounding the inner core, keeping the velocity jump at the inner core fixed or increasing it at most by 0.14 km/s in order to satisfy the amplitude data, (2) by decreasing the radius of the inner core, or (3) by decreasing the average velocity in the inner core by 0.5–0.1 km/s, again honoring the velocity jump at the boundary. Only the last alternative would be consistent with the *PKiKP-PcP* data which, as they stand, suggest the reverse of options (1) and (2).

The differential time *PKiKP-PcP* (Table 11) is a measure of the radius of the inner core. Model C2 averages 0.6 s slower than the data of *Engdahl et al.* [1974]. On the assumption that core velocities in C2 are accurate this suggests that the inner core is 3 km larger than C2, or 1218 km. The scatter in the data, however, is such (−1.4 to +0.2 s) that inner core radii from 1214 to 1222 km are acceptable. The uncertainty in *PcP* and *PKP*, i.e., average velocities in the mantle, core, and outer core radius, is such that the value 1227.4 ± 0.6 km, preferred by *Engdahl et al.* [1974], is an acceptable solution, although their error estimate appears to be optimistic. An uncertainty in outer core travel times of 1 s immediately introduces an error of 5 km in the radius of the inner core.

Shear Waves

The scatter in shear wave travel times is well known. Part of the difficulty is related to the fact that shear waves are not first arrivals but must be picked out of the *P* coda; transformation

TABLE 6. Compressional Wave Travel Times and Errors

Δ, deg	JB	HCR	1968	C2	Difference JB	Difference HCR	Difference 1968
30	372.5	371.0	368.5	370.9	1.6	0.1	−2.4
35	416.1	414.8	413.3	415.3	0.8	−0.5	−2.0
40	458.1	457.0	455.7	457.8	0.3	−0.8	−2.1
45	498.9	497.4	496.4	498.4	0.5	−1.0	−2.0
50	538.0	536.1	535.2	537.0	1.0	−0.9	−1.8
55	575.4	573.0	572.2	573.7	1.7	−0.7	−1.5
60	610.7	608.2	607.4	608.7	2.0	−0.5	−1.3
65	644.0	641.6	640.9	642.1	1.9	−0.5	−1.2
70	675.4	673.1	672.7	673.6	1.8	−0.5	−1.4
75	705.0	702.9	702.6	703.3	1.7	−0.4	−0.7
80	732.7	730.8	730.6	731.4	1.3	−0.6	−0.8
85	758.5	756.9	756.6	757.7	0.8	−0.8	−1.1
90	782.7	781.1	780.7	782.1	0.6	−1.0	−1.4
95	805.7		803.9	805.4	0.3		−1.5
Average difference					+1.2	−0.6	−1.5

Travel times are in seconds. JB denotes *Jeffreys and Bullen* [1940]; HCR, *Hales et al.* [1968]; and 1968, *Herrin et al.* [1968].

TABLE 7. Observed and Computed $dt/d\Delta$ of P Waves

Δ, deg	HCR	CGJ	LJ	DJC*	C2
30	8.94	8.88	8.92	9.13 ± 0.05	8.99
35	8.60	8.67	8.60	8.70 ± 0.05	8.67
40	8.26	8.30	8.38	8.26 ± 0.07	8.32
45	7.91	7.99	7.90	8.11 ± 0.10	7.93
50	7.56	7.52	7.51	7.52 ± 0.10	7.53
55	7.21	7.10	7.22	7.19 ± 0.08	7.17
60	6.86	6.84	6.75	6.95 ± 0.07	6.83
65	6.50	6.66	6.53	6.69 ± 0.08	6.49
70	6.14	6.17	6.24	6.21 ± 0.09	6.13
75	5.77	5.77	5.83	5.88 ± 0.06	5.78
80	5.40	5.35	5.48	5.47 ± 0.06	5.44
85	5.03	4.98	4.93	4.95 ± 0.06	5.06
90	4.66	4.74	4.65	4.60 ± 0.09	4.75
95	4.28	4.55	4.48	4.52 ± 0.07	4.57

Values for $dt/d\Delta$ are in seconds per degree. HCR denotes *Hales et al.* [1968]; CGJ, *Carder et al.* [1966]; LJ, *Johnson* [1969]; and DJC, *Corbishley* [1970].
*Uncertainty is 95% confidence interval.

TABLE 8. *PcP* Times and Errors

Δ, deg	JB	Gogna	68M	C2	Difference JB	Difference Gogna	Difference 68M
30	554.9	553.0	551.1	552.2	2.7	0.8	−1.1
35	568.6	567.4	564.9	566.1	2.5	1.3	−1.2
40	583.9	583.2	580.3	581.4	2.5	1.8	−1.1
45	600.5	600.2	596.9	598.1	2.4	2.1	−1.2
50	618.3	618.2	614.8	616.0	2.3	2.2	−1.2
55	637.0	636.8	633.7	634.9	2.1	1.9	−1.2
60	656.6	656.0	653.3	654.6	2.0	1.4	−1.3
65	676.9	675.9	673.7	675.0	1.9	0.9	−1.3
70	697.8	695.6	694.7	696.0	1.8	−0.4	−1.3
75	719.1	716.0	716.1	717.4	1.7	−1.4	−1.3
80	740.6	737.1	737.8	739.1	1.5	−2.0	−1.3
85	762.3	759.2	759.7	761.1	1.2	−1.9	−1.4
90	784.2	781.6	781.8	783.3	0.9	−1.7	−1.5
Average difference					+2.0	+0.3	−1.3

Values are in seconds. JB denotes *Jeffreys and Bullen* [1940]; Gogna, *Gogna* [1973]; and 68M, *Engdahl and Johnson* [1974].

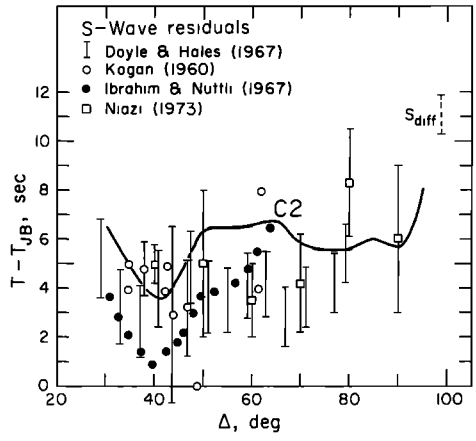

Fig. 4. Shear velocity residual, relative to the Jeffreys-Bullen (JB) tables, of C2 and other recent studies.

of *S* to *P* at upper mantle and crustal discontinuities can also bias '*S* readings' toward earlier arrivals. Shear waves are much longer in period than *P* waves and suffer more attenuation. They are also not efficiently generated by underground explosions. All of the above facts combine to make shear wave arrival times at least 4 times more uncertain than *P* wave arrival times. In addition, there seem to be real lateral variation effects, including source, path, and receiver variations, that are more pronounced for *S* waves than for *P* waves. Additional complications include large-amplitude surface reflections and interference by *PL* waves [*Helmberger and Engen,* 1974].

In comparison with published *S* wave travel times (Table 12), C2 is 4.4–5.9 s slow between 30° and 95°. In comparison with unpublished data of F. E. Followill and O. Nuttli (1971), appropriate for paths to the western United States (tectonic), C2 is, on the average, 0.5 s slow. For other paths the discrepancy varies from about 5 s at 35° to 3 s at 95°. From about 30°–40°, C2 agrees with data of *Kogan* [1960] for Pacific surface explosions and falls between 'continental' and 'tectonic' solutions. Beyond 40°, C2 is 2–4 s slow in comparison with most shear wave travel times. Some of the data reported by *Kogan* [1960], *Niazi* [1973], and *Bolt et al.* [1970] are even slower than C2. However, studying the data, one gets the impression that C2 is slow by 2–4 s in comparison with the majority of shear wave travel time studies.

Between 30° and 45° and 75° and 80° (Table 12) the shear wave travel times are bracketed by body wave solutions. Outside these regions, C2 is at least 2.2 s slow in comparison with body wave data. The calculated $dt/d\Delta$ for shear waves is generally consistent with observed values except possibly between 45°–50°. This is the region where data of *Hart* [1975] indicates revisions of earlier solutions.

ScS times are even less studied than *S* times. Model C2 is 6.0 s slower than JB or Gogna times. This is consistent with C2 *S* times, which are 4.5–5.9 slower than JB and Gogna times. The *S* and *ScS* data are therefore reasonably consistent with the view that average shear wave travel times in the mantle are about 4 s slower than standard body wave solutions. This can be compared with the earlier conclusions that the average earth is 0.6 s slower for *P* waves than obtained for that part of the earth available for *P* wave inspection.

The scatter in measured *ScS-S* times is 5–10 s [*Hales and Roberts,* 1970; *Jordan,* 1972; *Jordan and Lynn,* 1974]. This has been attributed to lateral variations in mantle *S* times [*Jordan and Lynn,* 1974] deep in the mantle. The average residual (*ScS-*

TABLE 10. *PKP* Times (Surface Focus) and Errors

Δ, deg	JB	68	JW	C2	Difference JB	Difference 68	Difference JW
170A	1286.3	1283.7		1284.7	1.6	−1.0	···
160	1242.7	1239.7	1241.8	1240.5	2.2	−0.8	1.3
150	1200.2	1196.9	1199.2	1197.7	2.5	−0.8	1.5
145B	1180.4	1178.0	1179.4	1177.7	2.7	+0.3	1.7
145B	1179.3	1174.4	1178.9	1176.7	2.6	−2.3	2.2
150	···	1188.1	1192.6	1190.1	···	−2.0	2.5
155C	···	1201.0	1204.1	1201.4	···	−0.4	2.7
122D			1136.8	1134.7			2.1
125			1142.7	1140.5			2.2
130	1152.0	1151.3	1152.5	1150.2	1.8	1.1	2.3
140	1170.5	1170.1	1171.2	1169.3	1.2	0.8	2.1
150	1187.4	1186.8	1188.0	1185.9	1.5	0.9	2.1
160	1200.8	1200.0	1201.5	1199.3	1.5	0.7	2.2
170	1209.2	1208.4	1210.4	1208.3	1.1	0.1	2.1
180F	1212.2	1211.0	1213.6	1211.8	0.4	−0.8	1.8
Average difference					+1.7	−0.3	+2.1
$P_{AB}' - P_{DF}'$							
170	77.1	75.3	···	76.4	0.7	−1.1	···
160	41.9	39.7	40.3	41.2	0.7	−1.5	−0.9
150	12.8	10.1	11.2	11.8	1.0	−1.7	−0.6
$P_{BC}' - P_{DF}'$, 150	···	1.3	4.6	4.2	···	−2.9	+0.4

JB denotes *Jeffreys and Bullen* [1940]; 68, *Herrin et al.* [1968]; and JW, *Whitcomb* [1973].

TABLE 9. *PcP-P* Times (Surface Focus) and Errors

Δ, deg	TJ	68M	C2	Error
30	181.9 ± 0.4	181.6 ± 0.6	181.3	0.3
35	151.4 ± 0.3	151.6 ± 0.6	150.8	0.8
40	125.1 ± 0.5	124.6 ± 0.6	123.6	1.0
45	100.7 ± 0.4	100.5 ± 0.6	99.7	0.8
50	79.9 ± 0.4	79.6 ± 0.6	79.0	0.6
55	62.3 ± 1.0	61.5 ± 0.6	61.2	0.3
60	46.1 ± 1.0	45.9 ± 0.6	45.9	0.0
65	33.0 ± 1.0	32.8 ± 0.6	32.9	−0.1
70	22.0 ± 2.7	22.0 ± 0.6	22.4	−0.4
75	13.4 ± 2.1	13.5 ± 0.6	14.1	−0.6
80		7.2 ± 0.6	7.7	−0.5
85		3.1 ± 0.6	3.4	−0.3
90		1.1 ± 0.6	1.2	−0.1

TJ denotes *Jordan* [1973], and 68M denotes *Engdahl and Johnson* [1974].

TABLE 11. *PKiKP-PcP* Times

Δ, deg	EFM	C2	Error
10.90	477.5	478.3	−0.8
11.73	477.2	477.6	−0.4
21.34	464.9	466.3	−1.4
26.64	457.4	457.7	−0.3
27.71	454.8	455.7	−0.9
29.69	451.2	452.1	−0.9
30.50	450.4	450.5	−0.1
30.60	449.5	450.3	−0.8
31.08	448.2	449.3	−1.1
35.94	438.4	439.1	−0.7
36.04	438.8	438.9	−0.1
38.17	433.5	433.3	+0.2
47.18	411.9	412.1	−0.2
Mean error			−0.6

Values are in seconds. EFM denotes *Engdahl et al.* [1974].

TABLE 12. Shear Wave Travel Times (Surface Focus) and $dt/d\Delta$

Δ, deg	JB	FEF	HR	C2	$dt/d\Delta$, s/deg HR	FEF	C2
30	670.2	680.0	669.5	676.7	15.4	16.0	15.5
35	748.2	757.2	749.0	753.1	15.3	15.3	15.2
40	824.5	831.5	825.7	821.1	15.2	14.6	14.9
45	897.9	902.3	899.5	902.4	14.5	14.1	14.8
50	968.6	972.5	970.5	975.0	13.9	13.8	14.5
55	1036.8	1041.1	1038.7	1043.2	13.4	13.3	13.4
60	1102.6	1106.5	1104.1	1109.2	12.8	12.9	13.0
65	1165.5	1169.5	1166.7	1172.2	12.2	12.3	12.1
70	1225.6	1229.9	1226.4	1231.4	11.7	11.9	11.6
75	1282.6	1288.1	1283.2	1288.1	11.1	11.1	11.1
80	1336.5	1341.9	1337.3	1342.1	10.5	10.3	10.6
85	1387.3	1391.2	1388.5	1393.3	10.0	9.7	9.9
90	1435.5	1438.9	1436.9	1441.1	9.4	9.2	9.2
95	1478.2	1484.0	1482.4	1486.0	8.8	8.8	8.8

JB denotes *Jeffreys and Bullen* [1940]; FEF, F. E. Followill and O. Nuttli (personal communication, 1971); and HR, *Hales and Roberts* [1970].

$S)_{C2} - (ScS\text{-}S)_{JB}$ over the distance range 30°–80° is +0.7s for deep focus events. The *Jordan* [1972] data set gives $+1.7 \pm 1.3$ s (95% confidence interval). Between 40° and 70°, C2 has a JB residual of +0.4 s compared with the *Jordan* [1972] value +0.5 s. The *ScS-S* data are summarized in Table 13. We conclude that C2 is an adequate fit to the *ScS-S* data.

Composition of the Mantle

Burdick and Anderson [1975] showed that the major features of the upper mantle and transition region could be accounted for by an olivine-rich mantle undergoing phase changes to β spinel near 400 km and γ spinel near 500 km. Some pyroxene was required in order to satisfy the densities and to make the fayalite content of the olivine more in line with petrologic estimates. The mantle between the base of the LVZ and 600 km appeared to be chemically homogeneous. The 650-km discontinuity appears to be the result of the transformation of pyroxene-garnet to oxides or perovskite (D. L. Anderson, in preparation, 1976). The lower mantle has properties consistent with the properties of the mixed oxides (Fe, Mg)O + SiO_2 (stishovite). *Anderson and Sammis* [1970] concluded from earlier earth models that the LVZ was due to partial melting and that small amounts of water were required in order to depress the melting point. All of these conclusions are consistent with the new earth model. The structure below 670 km indicates further phase changes, possibly involving ilmenite, perovskite, and mixed oxide assemblages. The lower mantle between depths of about 1500 and 2600 km is relatively homogeneous. Velocity gradients, and possibly the density gradient, in the lowermost 300 km of the mantle are less than in the rest of the lower mantle. This could be due to temperature or compositional gradients in this region. A high temperature gradient could result from heating by the core. The core efficiently brings heat to the base of the mantle both by conduction and by convection, but heat is not easily transported across the boundary because of the more insulating nature of silicates. A high temperature gradient at the base of the mantle is therefore to be expected. The U and Th content at the base of the mantle may also be high [*Anderson*, 1972, 1975; *Anderson and Hanks*, 1972]. There is also the possibility that the bulk chemistry of this region is more refractory than is that of the normal mantle [*Anderson*, 1972].

TABLE 13. *ScS-S* Travel Times

Δ, deg	JA*	C2	Difference
30	311.3 ± 1.8	306.8	−4.5
35	259.4 ± 1.5	258.3	−1.1
40	215.7 ± 1.6	213.3	−2.4
45	174.3 ± 1.1	172.2	−2.1
50	138.6 ± 1.4	137.9	−0.8
55	108.5 ± 1.3	107.2	−1.3
60	82.0 ± 1.1	80.7	−1.3
65	59.7 ± 0.9	59.2	−0.5
70	40.6 ± 1.0	41.2	−0.6
75	25.5 ± 1.3	26.6	1.1
80	14.0 ± 0.8	15.1	1.1

JA denotes *Jordan and Anderson* [1974].
*Uncertainty is 95% confidence interval.

The uppermost mantle, the lid of the low-velocity zone, does not fall on any reasonable extrapolation of the 250- to 300-km region of the mantle. The velocities in the lid are greater than in olivine or pyroxene and must contain substantial portions of spinel or garnet or some other dense phase. The velocities and density are appropriate for eclogite. The closest match is with an eclogite from Nordfjord, Norway, which has 24% orthopyroxene, 23% clinopyroxene, and 51% garnet [*Manghnani et al.*, 1974]. *Press* [1969] has also suggested that eclogite may be an important component of the upper mantle. These conclusions are based partly on the evidence from body wave studies for high velocities in the lithosphere, since the normal mode data set has limited resolving power in this region of the mantle.

Summary

An earth model based on high-resolution body wave studies has been inverted with the use of a representative set of 400 normal mode periods including many higher modes. The resulting model, designated C2, satisfies the free oscillation data with an average error of about 0.08%. It is also in agreement with a large body of travel time, apparent velocity, and differential travel time data. Although there is a large spread in body wave solutions, there is a suggestion that the average earth, mainly oceans, is slightly slower than that part of the earth available for body wave inspection, mainly tectonic to continental paths.

Model C2 has pronounced low-velocity zones for both *P* and *S*, a relatively high-density and high-velocity upper mantle lid, and transition regions near 375–425, 500–550, and 650–675 km. There is also moderate structure between 700 and 1200 km and slight inhomogeneity on both sides of the mantle-core and outer core–inner core boundaries. The V_p and density jump at the outer core–inner core boundary is small. The radius of the inner core is probably slightly larger than the 1215 km given by the model.

The uppermost mantle is consistent with eclogite overlying a thick partially molten zone. The rest of the upper mantle is consistent with olivine and pyroxene and their successive transformation to higher-pressure assemblages.

Acknowledgments. This research was supported by the Advanced Research Projects Agency of the Department of Defense and was monitored by the Air Force Office of Scientific Research under contract F44620-72-C-0078. Tom Jordan participated extensively in the early part of this study, and we are indebted to him for much advice. We would like to thank F. Gilbert, A. Dziewonski, D. Helmberger, and B. Bolt for preprints of their papers. Conversations with Martin Smith and Freeman Gilbert were quite helpful. One of us (R.S.H.) thanks the National Science Foundation for graduate fellowship

support. Contribution 2637 of the Division of Geological and Planetary Sciences, California Institute of Technology, Pasadena, California 91125.

REFERENCES

Anderson, D. L., Phase changes in the upper mantle, *Science, 157,* 1165, 1967*a*.

Anderson, D. L., Latest information from seismic observations, *The Earth's Mantle,* edited by T. F. Gaskell, p. 355, Academic, New York, 1967*b*.

Anderson, D. L., Implications of the inhomogeneous planetary accretion hypothesis, *Comments Earth Sci. Geophys. 2,* 93, 1972.

Anderson, D. L., Chemical plumes in the mantle, *Geol. Soc. Amer. Bull., 86,* 1593, 1975.

Anderson, D. L., and T. C. Hanks, Formation of the Earth's core, *Nature, 237,* 387, 1972.

Anderson, D. L., and C. Sammis, Partial melting in the upper mantle, *Phys. Earth Planet. Interiors, 3,* 41, 1970.

Anderson, D. L., and M. N. Toksöz, Surface waves on a spherical earth, 1, Upper mantle structure from Love waves, *J. Geophys. Res., 68,* 3483, 1963.

Backus, G., and F. Gilbert, The resulting power of gross earth data, *Geophys. J. Roy. Astron. Soc., 16,* 169–205, 1968.

Bolt, B. A., and R. G. Currie, Maximum entropy estimates of Earth torsional eigenperiods from 1960 Trieste data, *Geophys. J. Roy. Astron. Soc., 40,* 107, 1975.

Bolt, B. A., M. Niazi, and M. Sommerville, Diffracted *ScS* and the shear velocity at the core boundary, *Geophys. J. Roy. Astron. Soc., 19,* 299, 1970.

Brune, J. N., and F. Gilbert, Torsional overtone dispersion from correlations of *S* waves to *SS* waves, *Bull. Seismol. Soc. Amer., 64,* 313, 1974.

Burdick, L. J., and D. L. Anderson, Interpretation of velocity profiles of the mantle, *J. Geophys. Res., 80,* 1070, 1975.

Carder, D. S., D. W. Gordon, and J. N. Jordan, Analysis of surface-foci travel times, *Bull. Seismol. Soc. Amer., 56,* 815, 1966.

Cleary, J. R., and A. L. Hales, An analysis of the travel times of *P* waves to North American stations in the distance range of 32° to 100°, *Bull. Seismol. Soc. Amer., 56,* 467, 1966.

Corbishley, D. J., Multiple array measurements of the *P*-wave travel-time derivative, *Geophys. J. Roy. Astron. Soc., 19,* 1, 1970.

Derr, J. S., Free oscillation observations through 1968, *Bull. Seismol. Soc. Amer., 59,* 2079, 1969.

Doyle, H. A., and A. L. Hales, An analysis of the travel times of *S* waves to North American stations in the distance range 28° to 82°, *Bull. Seismol. Soc. Amer., 57,* 761, 1967.

Dziewonski, A., On regional differences in dispersion of mantle Rayleigh waves, *Geophys. J. Roy. Astron. Soc., 22,* 289, 1971.

Dziewonski, A., and F. Gilbert, Observations of normal modes from 84 recordings of the Alaskan earthquake of 1964, March 28, *Geophys. J. Roy. Astron. Soc., 27,* 393, 1973.

Dziewonski, A., J. Mills, and S. Bloch, Residual dispersion measurement—A new method of surface wave analysis, *Bull. Seismol. Soc. Amer., 62,* 129, 1972.

Dziewonski, A., A. L. Hales, and E. R. Lapwood, Parametrically simple earth models consistent with geophysical data, *Phys. Earth Planet. Interiors, 10,* 12, 1975.

Engdahl, E. R., and E. A. Flinn, Seismic waves reflected from discontinuities within the upper mantle, *Science, 163,* 177, 1969.

Engdahl, E. R., and L. E. Johnson, Differential *PcP* travel-times and the radius of the core, *Geophys. J. Roy. Astron. Soc., 39,* 435, 1974.

Engdahl, E. R., E. A. Flinn, and R. P. Masse, Differential *PKiKP* travel-times and the radius of the inner core, *Geophys. J. Roy. Astron. Soc., 39,* 457, 1974.

Gilbert, F., and A. Dziewonski, An application of normal mode theory to the retrieval of structural parameters and source mechanisms from seismic spectra, *Phil. Trans. Roy. Soc. London. Ser. A, 278,* 187, 1975.

Gilbert F., A. Dziewonski, and J. Brune, An informative solution to a seismological inverse problem, *Proc. Nat. Acad. Sci. U. S. A., 70,* 1410–1413, 1973.

Gogna, M. L., Travel times of *S*, *PcP*, and *ScS* from Pacific earthquakes, *Geophys. J. Roy. Astron. Soc., 33,* 103, 1973.

Hales, A. L., Eigenperiods of earth models and the determination of travel-time baselines, *J. Geophys. Res., 79,* 422, 1974.

Hales, A. L., and J. L. Roberts, Shear velocities in the lower mantle and the radius of the core, *Bull. Seismol. Soc. Amer., 60,* 1427, 1970.

Hales, A. L., J. R. Cleary, and J. L. Roberts, Velocity distributions in the lower mantle, *Bull. Seismol. Soc. Amer., 58,* 1975, 1968.

Hart, R. S., Shear velocity in the lower mantle from explosion data, *J. Geophys. Res., 80,* 4889, 1975.

Hart, R. S., and F. Press, S_n velocities and the composition of the lithosphere in the regionalized Atlantic, *J. Geophys. Res., 78,* 407–411, 1973.

Helmberger, D. V., and G. R. Engen, Upper mantle shear structure, *J. Geophys. Res., 79,* 4017, 1974.

Helmberger, D. V., and R. A. Wiggins, Upper mantle structure of middlewestern United States, *J. Geophys. Res., 76,* 3229, 1971.

Herrin, E. (chairman), 1968 seismological tables for *P* phases, *Bull. Seismol. Soc. Amer., 58,* 1193, 1968.

Ibrahim, A. K., and O. Nuttli, Travel-time curves and upper mantle structure from long period *S* waves, *Bull. Seismol. Soc. Amer., 57,* 1063, 1967.

Jeffreys, H., and Bullen, K. E., *Seismological Tables,* 55 pp., British Association for the Advancement of Science, London, 1940.

Johnson, L. R., Array measurements of *P* velocities in the upper mantle, *J. Geophys. Res.,* 72, 6309–6325, 1967.

Jordan, T. H., Estimation of the radial variation of seismic velocities and density in the earth, Ph.D. thesis, Calif. Inst. of Technol., Pasadena, 1972.

Jordan, T. H., and D. L. Anderson, Earth structure from free oscillations and travel times, *Geophys. J. Roy. Astron. Soc., 36,* 411, 1974.

Jordan, T. H., and W. S. Lynn, A velocity anomaly in the lower mantle, *J. Geophys. Res., 79,* 2679, 1974.

Julian, B. R., and D. L. Anderson, Travel times, apparent velocities and amplitudes of body waves, *Bull. Seismol. Soc. Amer., 58,* 339–366, 1968.

Kanamori, H., Velocity and *Q* of mantle waves, *Phys. Earth Planet. Interiors, 2,* 259, 1970.

Kogan, S. D., Travel times of longitudinal and transverse waves calculated from data on nuclear explosions made in the region of the Marshall Islands, *Izv. Acad. Sci. USSR Phys. Solid Earth,* Engl. Transl., no. 3, 242, 1960.

Kosminskaya, I. P., N. N. Puzyrev, and A. S. Aleks-eyev, Explosion seismology: Its past, present and future, *Tectonophysics, 13,* 309–324, 1972.

Manghnani, M. H., R. Ramananantoandro, and S. P. Clark, Compressional and shear wave velocities in granulite facies rocks and eclogites to 10 kbar, *J. Geophys. Res., 79,* 5427, 1974.

Mendiguren, J. A., Identification of the free oscillation spectra peaks for 1970 July 31, Columbian deep shock using the excitation criterion, *Geophys. J. Roy. Astron. Soc., 33,* 281, 1973.

Müller, G., Amplitude studies of core phases, *J. Geophys. Res., 78,* 3469, 1973.

Niazi, M., and D. L. Anderson, Upper mantle structure of western North America from apparent velocities of *P* waves, *J. Geophys. Res., 70,* 4633, 1965.

Niazi, M., *SH* travel times and lateral heterogeneities in the lower mantle, *Bull. Seismol. Soc. Amer., 63,* 2035, 1973.

Press, F., The suboceanic mantle, *Science, 165,* 174–176, 1969.

Simpson, D. W., *P* wave velocity structure of the upper mantle in the Australian region, Ph.D. thesis, Aust. Nat. Univ., Canberra, 1973.

Sutton, G. H., and D. A. Walker, Oceanic mantle phases recorded on seismographs in the northwestern Pacific at distances between 7° and 40°, *Bull. Seismol. Soc. Amer., 62,* 631, 1972.

Whitcomb, J. H., A study of the velocity structure of the Earth by the use of core phases, *1*, Ph.D. thesis, Calif. Inst. of Technol., Pasadena, 1973.

Whitcomb, J. H., and D. L. Anderson, Reflection of *P'P'* (*PKPPKP*) seismic waves from discontinuities in the mantle, *J. Geophys. Res., 75,* 5713, 1970.

(Received June 9, 1975;
revised October 14, 1975;
accepted November 7, 1975.)